


Age and nature of the Jurassic–Early Cretaceous mafic and ultramafic rocks from the Yilashan area, Bangong–Nujiang suture zone, central Tibet: implications for petrogenesis and tectonic Evolution

Yun Zhong, Xi-Chong Hu, Wei-Liang Liu, Bin Xia, Xiao Zhang, Wei Huang, Yuan-Bin Fu & Yu-Guang Wang

To cite this article: Yun Zhong, Xi-Chong Hu, Wei-Liang Liu, Bin Xia, Xiao Zhang, Wei Huang, Yuan-Bin Fu & Yu-Guang Wang (2017): Age and nature of the Jurassic–Early Cretaceous mafic and ultramafic rocks from the Yilashan area, Bangong–Nujiang suture zone, central Tibet: implications for petrogenesis and tectonic Evolution, International Geology Review, DOI: [10.1080/00206814.2017.1385033](https://doi.org/10.1080/00206814.2017.1385033)

To link to this article: <http://dx.doi.org/10.1080/00206814.2017.1385033>

 View supplementary material 

 Published online: 13 Oct 2017.

 Submit your article to this journal 

 Article views: 4





 View related articles 

 View Crossmark data 

ARTICLE



Age and nature of the Jurassic–Early Cretaceous mafic and ultramafic rocks from the Yilashan area, Bangong–Nujiang suture zone, central Tibet: implications for petrogenesis and tectonic Evolution

Yun Zhong ^a, Xi-Chong Hu ^{b,c}, Wei-Liang Liu ^{c,d,e}, Bin Xia ^{c,d,e,f}, Xiao Zhang ^{c,d,e}, Wei Huang^g, Yuan-Bin Fu^b and Yu-Guang Wang^b

^aSchool of Earth Science and Geological Engineering, Sun Yat-sen University, Guangzhou, China; ^bIsland Protection and Utilization Research Center, National Marine Environmental Monitoring Center, Dalian, China; ^cSchool of Marine Sciences, Sun Yat-sen University, Guangzhou, China; ^dKey Laboratory of Offshore Oil Exploration and Development of Guangdong Higher Education Institutes, Offshore Oil Exploration and Development Center, Sun Yat-sen University, Guangzhou, China; ^eGuangdong Provincial Key Laboratory of Marine Resources and Coastal Engineering, Sun Yat-sen University, Guangzhou, China; ^fState Key Laboratory of Ore Deposit Geochemistry, Chinese Academy of Sciences, Guiyang, China; ^gXizang Geological Survey Institute, Tibet Autonomous Region Geological And Mineral Exploration And Development Bureau, Lhasa, China

ABSTRACT

The Jurassic–Early Cretaceous Yilashan mafic–ultramafic complex is located in the middle part of the Bangong–Nujiang suture zone, central Tibet. It features a mantle sequence composed of peridotites and a crustal sequence composed of cumulate peridotites and gabbros that are intruded by diabases with some basalts. This article presents new whole-rock geochemical and geochronological data for peridotites, gabbros, diabases and basalts to revisit the petrogenesis and tectonic setting of the Yilashan mafic–ultramafic complex. Zircon laser ablation inductively coupled plasma mass spectrometer (LA-ICP-MS) U–Pb ages of three diabase samples are 169.6 ± 3.3 Ma, 132.5 ± 2.5 Ma, and 133.6 ± 4.9 Ma, respectively. These ages together with previous studies indicate that the Yilashan mafic–ultramafic complex probably formed during the Jurassic–Early Cretaceous. The peridotites exhibit nearly U-shaped REE patterns and are distinct from abyssal peridotites. The diabase and basalt samples show arc features with selective enrichment in light rare earth elements (LREE) and large ion lithophile elements (LILEs; e.g. Rb, U, and Sr) and depletion in high field strength elements (HFSEs; e.g. Nb, Ta, and Ti). The gabbro samples display cumulate features with selective enrichment in LILEs (e.g. Rb, Ba, and Sr) but depletion in LREEs and HFSEs (e.g. Nb, Zr, and Ti). Combining the positive $\epsilon_{Nd}(t)$ values (+6.1 to +10.0) and negative zircon $\epsilon_{Hf}(t)$ values (–16.5 to –11.7 and –13.6 to –0.4) with older Hf model ages for the mafic rocks, these signatures suggest that the Yilashan mafic and ultramafic rocks likely originated from an ancient lithospheric mantle source with the addition of asthenospheric mantle materials and subducted fluids coupled with limited crustal contamination in a continental arc setting as a result of the southward subduction of the Bangong–Nujiang Tethys Ocean beneath the Lhasa terrane during the Jurassic–Early Cretaceous.

ARTICLE HISTORY

Received 7 May 2017
Accepted 24 September 2017

KEYWORDS

Yilashan; mafic and ultramafic rocks; continental arc; LA-ICP-MS dating; geochemistry

1. Introduction

The Bangong–Nujiang suture zone (BNSZ) is one of the most important suture zones in the Tibetan Plateau (Figure 1(a)). It represents remnants of the vanished Bangong–Nujiang Tethys Ocean (BNTO) and constitutes the collision zone between the Qiangtang and Lhasa terranes. Multitudinous mafic and ultramafic rocks such as ophiolites have been identified in the BNSZ, provide useful information with respect to the origin and tectonic evolution of the BNTO and promote the understanding of the development of the Tibetan Plateau.

The BNSZ trends nearly E–W throughout the central Tibetan Plateau from Bangong Lake to Dinging and winds along with the Nujiang River in the SE direction to western Yunnan (Figure 1(b); Xiao and Li 2000). Generally, the BNSZ is divided into western (Bangong Lake–Gerze), central (Dongqiao–Amdo), and eastern (Dingqing–Nujiang) sections from west to east (Wang *et al.* 1987; Xiao and Li 2000). Mafic and ultramafic rocks in the central BNSZ are always the subject of intense study in the field of the BNSZ due to their wide distribution and significant implications for tectonic framework and evolution of the BNTO. For example, many

CONTACT Xi-Chong Hu  huxich@mail2.sysu.edu.cn; Bin Xia  xiabin08@outlook.com

 Supplemental data for this article can be accessed [here](#).

© 2017 Informa UK Limited, trading as Taylor & Francis Group

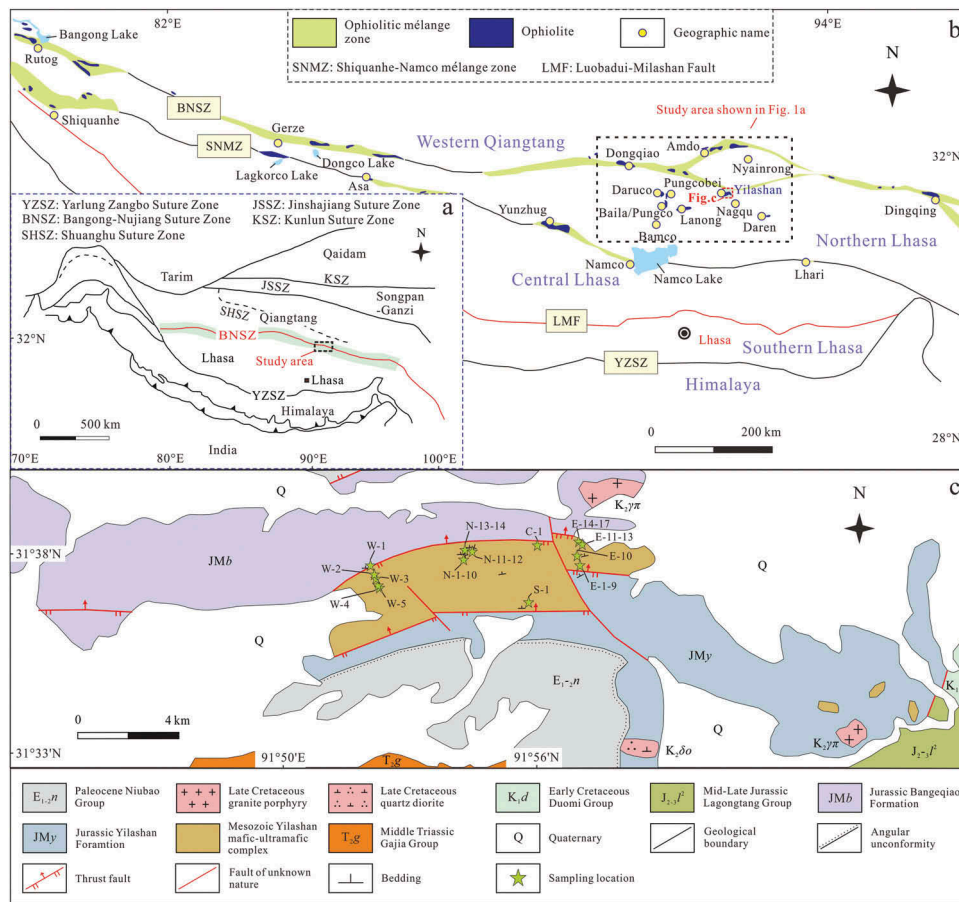


Figure 1. (a) Tectonic outline of the Qinghai-Tibet Plateau (after Zhang *et al.* 2004), (b) Sketch structural framework of the Lhasa terrane showing the Bangong-Nujiang suture zone (after Zhu *et al.* 2013); and (c) Simplified geological map of the Yilashan mafic-ultramafic complex (after Xizang Geological Survey Institute 2005).

previous studies on the geochemistry and geochronology of the central BNSZ ophiolites, which basically consist of mafic and ultramafic rocks, have been reported (Table 1). However, some essential problems are still in dispute, including the tectonic setting (small oceanic basin or wide oceanic basin), time of formation (e.g. initial opening or initial subduction of oceanic basin), subduction polarity of the oceanic basin (northward, southward or bidirectional subduction) and the tectonic model (e.g. intra-oceanic subduction or continental margin subduction) of these ophiolites are still in dispute (e.g. Wang *et al.* 1987, 2016; Pearce and Deng 1988; Zhu 2004; Pan *et al.* 2012; Zhang *et al.* 2012, 2014a, 2014b, 2017; Zhu *et al.* 2013; Chen *et al.* 2015; Zhang and Zhang 2017). These issues concern the basic interpretation of the generation of the central BNSZ and greatly restrict the understanding of the tectonic evolution of the BNTO.

Despite previous studies of the central BNSZ ophiolites having produced some controversies, the mafic and ultramafic rocks in this region remain the most effective means to resolve these basic problems noted

above due to their natural attributes. The Yilashan mafic-ultramafic complex in the Nagqu area occurs in the central BNSZ (Figure 1(b)). Generally, this complex is regarded as representative of ophiolite that belongs to the central section of the Bangong-Nujiang ophiolite belt (Pearce and Deng 1988; Huang *et al.* 2013). It features a mantle sequence composed of peridotites and a crustal sequence composed of cumulate peridotites and gabbros, which are intruded by diabases with some basalts (Figure 2), and acts as an ideal locale for studying the origin and tectonic evolution of the central BNSZ. Although previous studies involving petrography, geochemistry and geochronology have been reported (Table 1; e.g. Wang *et al.* 1987; Pearce and Deng 1988; Pan *et al.* 1997, 2006, 2012; Huang *et al.* 2013), the systematic geochemical and geochronological studies of the Yilashan mafic and ultramafic rocks are insufficient, such as the whole-rock Sr-Nd and zircon Lu-Hf isotopes of mafic rocks. Although a zircon LA-ICP-MS U-Pb age of 183.7 ± 1 Ma for gabbro has been reported (Huang *et al.* 2013), an ^{40}Ar - ^{39}Ar age of 114 ± 2 Ma on plagioclase for gabbro proposed by

Table 1. Summary of the geochemical characteristics, tectonic settings, and geochronological data of the ophiolites and the Yilashan mafic–ultramafic complex from the study area.

Location	Geochemical characteristics	Tectonic setting	Age (methods and dated material)	References
Amdo	SSZ	Back-arc basin; intra-oceanic subducted setting; intra-oceanic back- arc basin	188.0 ± 2.0 Ma (U–Pb zircon; plagiogranite); 184.0 ± 2.0 Ma (U–Pb zircon; gabbro); 220.0 ± 2.1 Ma (U–Pb zircon; gabbro)	Pearce and Deng (1988), Lai and Liu (2003), Sun <i>et al.</i> (2011), Wang <i>et al.</i> (2016), Chen <i>et al.</i> (2015)
Dongqiao	SSZ, OIB	Oceanic basin; back-arc basin; initial fore-arc basin; intra-oceanic subducted setting	187.8 ± 3.7 Ma (U–Pb zircon; gabbro); 187.0 ± 2.0 Ma (U–Pb zircon; gabbro); 188.4 ± 1.2 Ma (U–Pb zircon; gabbro); 181.4 ± 1.3 Ma (U–Pb zircon; gabbro); 145 Ma (K–Ar; basalt); 251 ± 65 Ma (Re–Os; cumulate rocks (harzburgite, wehrlite, and gabbro)	Wang <i>et al.</i> (1987, 2016), Pearce and Deng (1988), Ye <i>et al.</i> (2004), Xu <i>et al.</i> (2007), Xia <i>et al.</i> (2008), Shi <i>et al.</i> (2012), Liu <i>et al.</i> (2016)
Pungcobei	SSZ	Back-arc basin	188.1 ± 4.1 Ma (U–Pb zircon; gabbro)	Huang <i>et al.</i> (2015a)
Pungco (Baila)	SSZ	Fore-arc basin; back-arc basin	120 ± 1.4 Ma (K–Ar; basalt); 159.0 ± 2.1 Ma (U–Pb zircon; gabbro)	Wang <i>et al.</i> (1987, 2017), Pearce and Deng (1988), Chen <i>et al.</i> (2006), Wei <i>et al.</i> (2009)
Lanong	SSZ	Fore-arc setting; back-arc basin	128 Ma (U–Pb zircon; gabbro); 148.4 ± 1.7 Ma (U–Pb zircon; basalt); 149.1 ± 1.1 Ma (U–Pb zircon; gabbro diabase)	Wang <i>et al.</i> (1987), Pearce and Deng (1988), Chen <i>et al.</i> (2006), Xu <i>et al.</i> (2010), Zhong <i>et al.</i> (2017)
Yilashan	SSZ	Fore-arc setting; back-arc basin	183.7 ± 1 Ma (U–Pb zircon; gabbro); 114 ± 2 Ma (Ar–Ar plagioclase; gabbro)	Pearce and Deng (1988), Pan <i>et al.</i> (1997), Huang <i>et al.</i> (2013), Zhang <i>et al.</i> (2014a)
Daren	SSZ	Back-arc basin; inter- arc basin	259–242 Ma (U–Pb zircon; gabbro)	Chen <i>et al.</i> (2005)
Namco			166 ± 26 Ma (Rb–Sr; harzburgite); 178.0 ± 2.9 Ma (U–Pb zircon; gabbro); 149.7 ± 1.6 Ma (U–Pb zircon; gabbro)	Yang <i>et al.</i> (2003), Ye (2004), Zhong <i>et al.</i> (2015)

SSZ: supra-subduction zone; OIB: oceanic island basalt.

Zhang *et al.* (2014a) indicates that the Yilashan mafic–ultramafic complex likely experienced multiple igneous events. Meanwhile, Os isotopes of Cr-spinel in dunites suggest that the Yilashan mafic–ultramafic complex was derived from a weakly depleted asthenospheric mantle source (Huang *et al.* 2013). Similarly, Zhang *et al.* (2014a) proposed that basalts occurring in the central Tibetan Meso-Tethyan oceanic plateau (including the Yilashan basalts) have a plume mantle upwelling origin with an admixture of continental components (crust). However, Huang *et al.* (2015a) argued that the Yilashan harzburgites and dunites formed with the input of Mesoproterozoic lithospheric mantle components (sub-continental lithospheric mantle) based on the $^{187}\text{Os}/^{188}\text{Os}$ isotopic compositions. Moreover, whether the Yilashan mafic–ultramafic complex formed in a fore-arc setting (Pearce and Deng 1988) or a back-arc setting (e.g. Wang *et al.* 1987; Huang *et al.* 2013) or even an oceanic plateau setting (Zhang *et al.* 2014a) is still uncertain. In addition, whether the development of the Yilashan mafic–ultramafic complex was associated with the northward (Pearce and Deng 1988) or southward subduction of the Bangong–Nujiang Tethys Ocean or the northward

subduction of the Yarlung Zangbo Tethys Ocean (Wang *et al.* 1987; Zhang *et al.* 2004) is also under debate.

In this article, we present new whole-rock geochemical data, zircon LA-ICP-MS U–Pb ages and Lu–Hf isotopic data of mafic and ultramafic rocks from the Yilashan area. Based on the new data, we aim to constrain the petrogenesis, formation age and tectonic setting of the Yilashan mafic and ultramafic rocks and to discuss their significance in the tectonic evolution of the central BNSZ.

2. Geological background

The main body of the Tibetan Plateau consists of the Qaidam, Songpan–Ganzi, Qiangtang, Lhasa and Himalaya terranes from north to south in sequence (Figure 1(a)). The Lhasa terrane, located between the Yarlung Zangbo suture zone (YZSZ) and the BNSZ, plays a significant role in the formation of the Tibetan Plateau. Meso–Cenozoic igneous rocks and associated sediments are distributed widely in the Lhasa terrane (e.g. Zhu *et al.* 2009, 2011, 2013, 2016; Sui *et al.* 2013; Zhong *et al.* 2013; Kang *et al.* 2014; Chen *et al.* 2015; Hu *et al.* 2016; Zeng *et al.* 2016). This terrane can be divided into southern, central and northern terranes by the Luobadui–Milashan fault

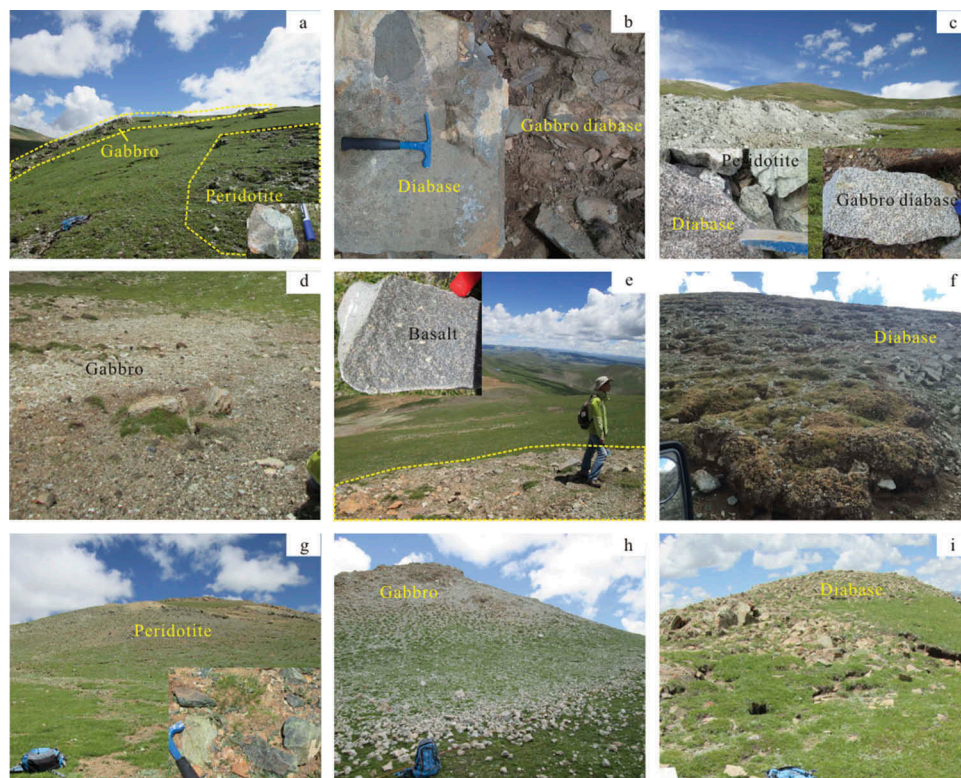


Figure 2. Field photographs of lithologic units of the Yilashan mafic–ultramafic complex. (a) E (eastern Yilashan mafic–ultramafic complex) serpentinized peridotite and gabbro; (b) E diabase and gabbro diabase; (c) N (northern Yilashan mafic–ultramafic complex) serpentinized peridotite, diabase, and gabbro diabase; (d) N gabbro; (e) S (southern Yilashan mafic–ultramafic complex) basalt (float); (f) C (central Yilashan mafic–ultramafic complex) diabase; (g) W (western Yilashan mafic–ultramafic complex) serpentinized peridotite; (h) W gabbro; and (i) W diabase.

(LMF) to the south and the Shiquanhe–Namco mélangé zone (SNMZ) to the north (Figure 1(b); Zhu *et al.* 2013). The central Lhasa terrane features an Archaean–Proterozoic metamorphic crystalline basement that was once to be an ancient microcontinent, whereas the southern and northern Lhasa terranes basically display younger and juvenile crustal characteristics related to the subduction of the Tethys Ocean (e.g. Mo *et al.* 2005; Chu *et al.* 2006; Pan *et al.* 2006, 2012; Zhu *et al.* 2008, 2016; Ji *et al.* 2009; Zhang *et al.* 2014b). In addition, the Amdo microcontinent to the north is characterized by Early Palaeozoic to Palaeoproterozoic metamorphic crystalline basement that likely was accreted instead of being a part of the Lhasa terrane (Figure 1(b); Zhu *et al.* 2009, 2011, 2013; Zhang *et al.* 2012, 2014c). It was probably an isolated block in the BNTO in the Permian–Triassic and subducted beneath the Qiangtang terrane (Zhang *et al.* 2014c) or the Amdo intra-oceanic back-arc basin (Chen *et al.* 2015) during the Early Jurassic. Two episodes of granitic magmatic activity, including a major one at 186–170 Ma (Guynn *et al.* 2006; Zhu *et al.* 2011; Dai *et al.* 2013) and a minor one at 140–110 Ma (Xu *et al.* 1985; Zhu *et al.* 2011; Dai *et al.* 2013), occurred in the Amdo terrane.

The BNSZ is located between the Qiangtang and Lhasa terranes in Tibet and is approximately 2000 km long and 20–200 km wide (Figure 1(b); Xiao and Li 2000; Yin and Harrison 2000). There are more than 80 ophiolitic massifs and associated tectonic mélanges in this suture zone (Bureau of Geology and Mineral Resources of Tibet 1993; Xiao and Li 2000). Ophiolites in the central BNSZ are arranged with a planar distribution (Figure 1(b)) comprising the Amdo, Dongqiao–Lunpola, Pungco (or Baila)–Lanong and Yunzhug–Namco subzones from north to south (Wang *et al.* 1987; Pearce and Deng 1988). As a whole, these ophiolites have complete rock assemblages but variable outcrop areas (e.g. Xiao and Li 2000; Xizang Geological Survey Institute 2003a, 2003b). Geochemical data show that the central BNSZ ophiolites were mainly generated in supra-subduction zone (SSZ) settings, including island arc, fore-arc, back-arc and inter-arc environments (Table 1; e.g. Pearce and Deng 1988; Wang *et al.* 2016; Chen *et al.* 2015; Zhong *et al.* 2015; Liu *et al.* 2016). These ophiolites display a broad range of formation ages from Triassic or earlier to Early Cretaceous but are clustered at Jurassic (Table 1; e.g. Wang *et al.* 2016, 2017; Chen *et al.* 2005, 2006, 2015; Xia *et al.* 2008; Sun *et al.* 2011; Huang *et al.* 2013, 2015b; Zhong

et al. 2015). These signatures, along with their sporadic distribution in the central BNSZ, imply that the central BNSZ ophiolites have a complex tectonic framework and evolutionary history (e.g. Pan *et al.* 2012; Zhu *et al.* 2013; Zhang *et al.* 2014a, 2014b).

The Yilashan mafic–ultramafic complex is situated approximately 20 km NW of Nagqu county (Figure 1 (b)) and shows the features of a tectonic *mélange*. It is mainly composed of peridotites and gabbros, and it is usually deemed to belong to the Pungco-Lanong ophiolitic subzone (Wang *et al.* 1987; Pearce and Deng 1988). Granophyres and quartz diorite porphyries occur locally in the complex as dikes. The mafic–ultramafic complex with a rhombic shape is basically surrounded by the Jurassic Mugagangri Group (JMy, JMb) with thrust faults on the northern and southern sides (Figure 1(c); Xizang Geological Survey Institute 2005). The Jurassic Mugagangri Group (JMy, JMb) exhibits the characteristics of flysch formation, with the Yilashan Formation (JMy) featuring ophiolitic tectonic *mélange* and the Bangeqiao Formation (JMb) occurring as deformed flysch sediments without exotic blocks (Xizang Geological Survey Institute 2005).

3. Petrography

3.1. Ultramafic rocks

Harzburgites have serpentinized olivine (75–80%) and orthopyroxene (10–15%) with minor Cr-spinel and carbonate. Orthopyroxene has been altered to serpentine pseudomorphs. Chrysanthemum-like carbonate aggregates are common that indicate carbonatization in a statics environment after serpentinization (Figure 3(a)).

Cumulate peridotites comprise serpentinized olivine (75–85%) and clinopyroxene (10–15%) with subordinate Cr-spinel, chlorite, and carbonate. Serpentinization of olivine and clinopyroxene is clear, but cribriform phenocrysts of clinopyroxene and olivine pseudomorphs are preserved. There are many Cr-spinels (2–3%) with approximate orientation and irregular distribution. Antigorite veins are present (Figure 3(b)).

3.2. Mafic rocks

Gabbros display a gabbroic texture and are characterized by euhedral to subhedral phenocrysts of clinopyroxene (<0.3 mm; 40–45%) and plagioclase (<0.3 mm; 50–60%) with subordinate prehnite and chlorite. Phenocrysts are broken. Clinopyroxenes have been variably altered into chlorite, and prehnitization in plagioclase is common (Figure 3(c and d)).

Diabases display ophitic, gabbro-diabasic and lamprophyric textures and are characterized by euhedral to subhedral hornblende (<0.6 mm; 40–50%), plagioclase (<0.3 mm; 35–40%) and pyroxene with subordinate epidote, sericite, prehnite, albite, quartz and carbonate. Amphibolization in pyroxene is common, and some hornblende phenocrysts exhibit relict crystals of pyroxene. Hornblende has been variably altered into carbonate, whereas plagioclase has experienced variable degrees of sericitization and carbonatization (Figure 3 (e)). Prehnitization and albitization in plagioclase are also common, and some prehnite and albite aggregations are distributed as veins. Small numbers of quartz grains occur as xenoliths or interstitial grains.

Basaltic porphyries exhibit a porphyritic texture, and contain euhedral to subhedral clinopyroxene (<0.1 mm; 30%) and plagioclase (<0.2 mm; 60%) with subordinate magnetite, biotite, carbonate and interstitial quartz. Clinopyroxene and plagioclase phenocrysts are very fresh. The number of plagioclase phenocrysts is greater than that of clinopyroxene phenocrysts. Biotite reaction rims have formed around the periphery of magnetite grains (Figure 3(f)).

4. Analytical methods

4.1. Whole-rock geochemical analysis

Thirty-eight representative samples of the Yilashan mafic and ultramafic rocks were selected for whole-rock geochemical analysis. The determination of whole-rock major element contents was conducted using an X-ray fluorescence (XRF) spectrometer at the Guangzhou ALS Chemex Company, China. The major method and procedure of analysis are described by Chen *et al.* (2014) and have analytical accuracies better than ± 1 –2%.

Whole-rock trace element data of the samples E-7 and C-1 were measured using ICP-MS at the Guangzhou ALS Chemex Company, China. The general methods and procedures are described by Chen *et al.* (2014) and have analytical precisions mostly better than ± 5 %. Whole-rock trace element compositions of other samples were determined using an ICP-MS at the State Key Laboratory of Ore Deposit Geochemistry, Chinese Academy of Sciences, China. The detailed methods and procedures are described by Qi and Grégoire (2000) and have measurement accuracies generally better than ± 5 %.

Whole-rock Sr–Nd isotopes of the samples E-8, E-14, N-4, and W-2 were analysed using a multi-collector MC-ICP-MS at the Speed Analysis & Testing Co., Ltd, Qingdao, China. The NBS 987 and Jndi-1 standard samples were used to monitor the measurement accuracy. The reported $^{87}\text{Sr}/^{86}\text{Sr}$ and $^{143}\text{Nd}/^{144}\text{Nd}$ ratios were

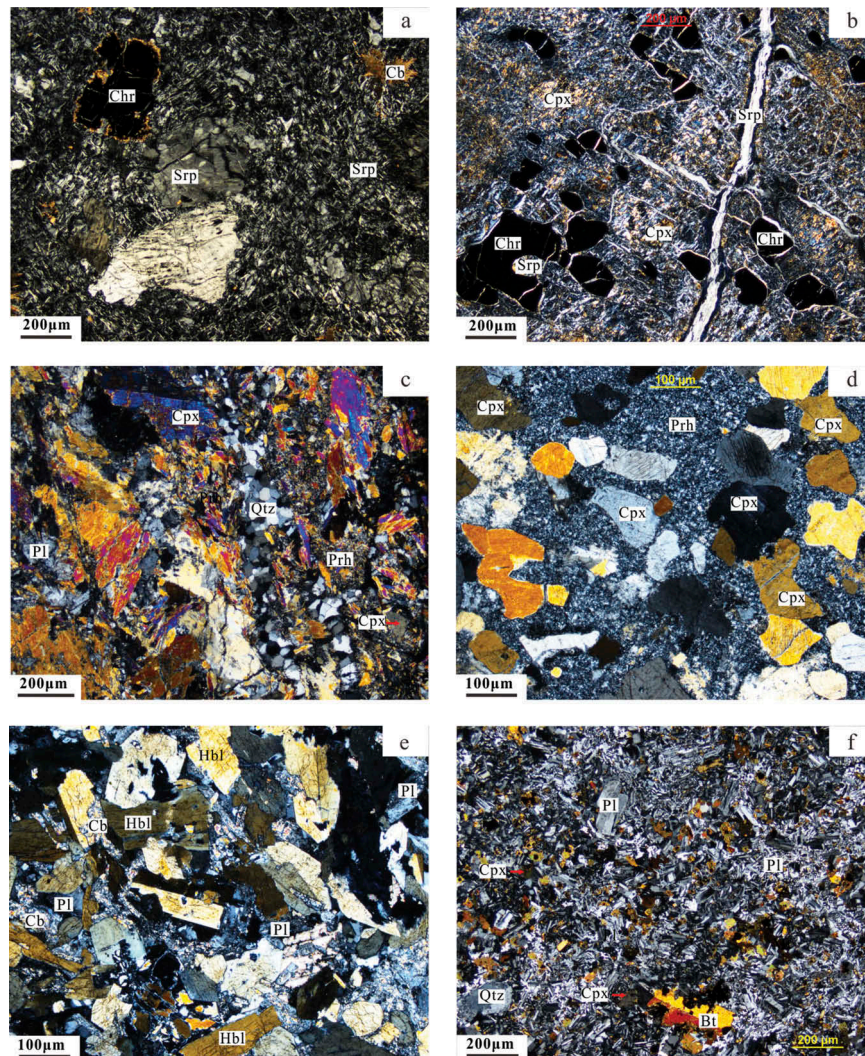


Figure 3. Representative photomicrographs of the Yilashan mafic and ultramafic rocks. (a) Sample W-1 harzburgite composed of serpentine, Cr-spinel and carbonate with pseudomorph of orthopyroxene; (b) Sample N-3 cumulate peridotite composed of serpentine, clinopyroxene and Cr-spinel with pseudomorph of olivine; (c) Mineral assemblage with quartz veins in sample E-10 gabbro; (d) Mineral assemblage of sample N-13 gabbro; (e) Mineral assemblage and ophitic texture of sample E-1 diabase porphyry; (f) Mineral assemblage of sample S-1 basalt porphyry. Srp: serpentine; Chr: chlorite; Cb: carbonate; Pl: plagioclase; Cpx: clinopyroxene; Hbl: hornblende; Prh: prehnite; Bt: biotite; Qtz: quartz.

normalized to $^{87}\text{Sr}/^{86}\text{Sr} = 0.1194$ and $^{143}\text{Nd}/^{144}\text{Nd} = 0.7219$ (Thirlwall 1991) for mass fractionation. The average $^{87}\text{Sr}/^{86}\text{Sr}$ ratio of the standard NBS 987 was 0.710295 ± 0.000007 (1σ , $N = 5$), and the average $^{143}\text{Nd}/^{144}\text{Nd}$ ratio of the standard Jndi-1 was 0.512085 ± 0.000005 (1σ , $N = 5$).

4.2. Zircon U–Pb and Lu–Hf isotopic composition

Zircon grains were obtained from samples E-6, N-7, and C-1 by the methods of heavy liquid and magnetic separation, and then representative grains were hand-picked using a binocular microscope. These grains were enclosed in epoxy resin and polished to expose their cores. Transmitted and reflected light and

cathodoluminescence (CL) images were photographed to display the external and internal structures and to identify appropriate spots for U–Pb and Lu–Hf isotopic analysis.

Zircon U–Pb dating was conducted at the State Key Laboratory of Isotope Geochemistry, Chinese Academy of Sciences. A 193-nm ArF-excimer laser ablation in combination with an Agilent 7500a LA-ICP-MS was used under the conditions of 32- μm spot diameter with a constant energy of 79 mJ/cm^{-2} at a repetition rate of 6 Hz. The detailed methods and procedures are described by Li *et al.* (2012). The standard silicate glass NIST SRM 610 was used to optimize U–Th–Pb concentrations, and the standard zircons TEMORA (E-6 and N-7) and 91,500 (C-1) were adopted as external standards to

calculate age. Off-line age calculations were performed using the EXCEL programs of ICPMSDataCal (Liu *et al.* 2008) and ISOPLOT (Ludwig 2003). Errors of all the individual analyses were reported at the 1σ level.

After zircon LA-ICP-MS U–Pb dating, zircon Lu–Hf isotopic compositions of samples E-6 and N-7 were analysed *in situ* on the dated spots at the State Key Laboratory of Isotope Geochemistry, Guangzhou Institute of Geochemistry, Chinese Academy of Sciences. A 193-nm ArF-excimer laser ablation attached to a Neptune plus multiple collector ICP-MS (LA-MC-ICP-MS) was used under the conditions of a spot diameter of 45 μm with an energy density of 80 mJ/cm^{-2} at 8-Hz repetition rate. The detailed analytical methods and procedures are described in Wu *et al.* (2006). The Penglai zircon was chosen as an external standard (Li *et al.* 2010). Zircon $\varepsilon_{\text{Hf}}(t)$ values were calculated relative to the ^{176}Lu decay constant ($1.867 \times 10^{-11} \text{ year}^{-1}$; Scherer *et al.* 2001) and the chondritic $^{176}\text{Lu}/^{177}\text{Hf}$ (0.0332) and $^{176}\text{Hf}/^{177}\text{Hf}$ (0.282772) ratios (Blichert and Albarede 1997). The single-stage Hf model age (T_{DM1}) was calculated with the present-day depleted mantle $^{176}\text{Lu}/^{177}\text{Hf}$ (0.0384) and $^{176}\text{Hf}/^{177}\text{Hf}$ (0.28325) ratios (Griffin *et al.* 2000), and the two-stage Hf model age (T_{DM2}) was calculated based on the $^{176}\text{Lu}/^{177}\text{Hf}$ ratio (0.015) of the average continental crust (Griffin *et al.* 2002).

5. Results

5.1. Zircon U–Pb ages

5.1.1 Sample E-6

Zircons selected from the diabasic sample E-6 are euhedral with prismatic shapes and range in size from 60 to 130 μm with length/width ratios of 1.5:1 to 3:1. The zircons show clear oscillatory zoning in CL images that indicate a magmatic origin (Figure 4(a)). Eleven spot analyses on 11 zircons (Figure 4(a)) show wide-ranging contents of U (389–1517 ppm) and Th (437–2351 ppm) with Th/U ratios of 0.5 to 1.6 (Supplementary Table 1). Note that most of the data plot away from the concordia curve (Figure 4(b)), which may be related to the Pb loss from zircon caused by later geological events (Wetherill 1956; Tilton 1960; Dickin 2005). The three most concordant spots have $^{206}\text{Pb}/^{238}\text{U}$ ages ranging from 169.1 ± 2.4 to 170.3 ± 3.5 Ma with a weighted mean age of 169.6 ± 3.3 Ma (MSWD = 0.05; Figure 4(b)).

5.1.2 Sample N-7

Zircons chosen from the diabasic sample N-7 are euhedral or broken crystals and exhibit prismatic shapes with grain sizes of 40–120 μm in length and length/

width ratios of 1:1 to 3:1. The zircon grains have clear oscillatory in CL images that suggest a magmatic origin (Figure 4(c)). Nine spot analyses on 9 zircons (Figure 4(c)) show the contents of U ranging from 109 to 528 ppm and Th from 62 to 511 ppm with Th/U ratios of 0.5 to 1.4 (Supplementary Table 1). Most of the data are concordant or near-concordant and yield $^{206}\text{Pb}/^{238}\text{U}$ ages ranging from 128.5 ± 3.6 to 134.9 ± 2.1 Ma with a weighted mean $^{206}\text{Pb}/^{238}\text{U}$ age of 132.5 ± 2.5 Ma (MSWD = 0.72; Figure 4(d)).

5.1.3 Sample C-1

Zircons obtained from the diabasic sample C-4 display euhedral or broken crystals with prismatic shapes and have lengths of 80–200 μm with length/width ratios of 2:1 to 3:1. The zircons exhibit oscillatory zoning in CL images, indicating a magmatic origin (Figure 4(e)). Ten spot analyses on 10 zircons (Figure 4(e)) have wide ranges of U (1302–10801 ppm) and Th (1067–6150 ppm) with Th/U ratios of 0.1–1.2 (Supplementary Table 1). Most of the data plot away from the concordia curve (Figure 4(f)), which may be associated with the Pb loss from zircon due to later geological events (Wetherill 1956; Tilton 1960; Dickin 2005). The two most concordant spots yield $^{206}\text{Pb}/^{238}\text{U}$ ages ranging from 132.8 ± 3.2 to 134.7 ± 3.9 Ma with a weighted mean age of 133.6 ± 4.9 Ma (MSWD = 0.13; Figure 4(f)).

5.2. Whole-rock geochemical compositions

The loss on ignition (LOI) contents of the Yilashan mafic and ultramafic rock samples range from 1.78 to 16.07 wt.% (Supplementary Table 2), indicating their various alterations. Thus, the major element compositions of these ultramafic-mafic rocks are recalculated to 100% (volatile free) in this article. Because the incompatible high field strength elements (HFSEs, e.g. Ta, Nb, and Ti), rare earth elements (REEs; e.g. La and Yb) and transition elements (e.g. Cr and Ni) are relatively immobile in the processes of severe seafloor-hydrothermal alteration and low- to medium-grade metamorphism (Bau 1991; Pearce and Cann 1973; Wood *et al.* 1979; Gibson *et al.* 1982), the geochemical discussions that follow are mainly based on these elements.

5.2.1 Ultramafic rocks

Nine representative whole-rock major and trace element analyses of the Yilashan peridotites (harzburgite and cumulate peridotite) are represented in Supplementary Table 2. The Yilashan peridotites have variable major element contents with SiO_2 ranging from 33.71 to 45.80 wt.%, Al_2O_3 from 0.16 to 4.09 wt.%, $\text{Fe}_2\text{O}_3\text{T}$ from 8.27 to 11.25 wt.%, MgO from 40.94 to

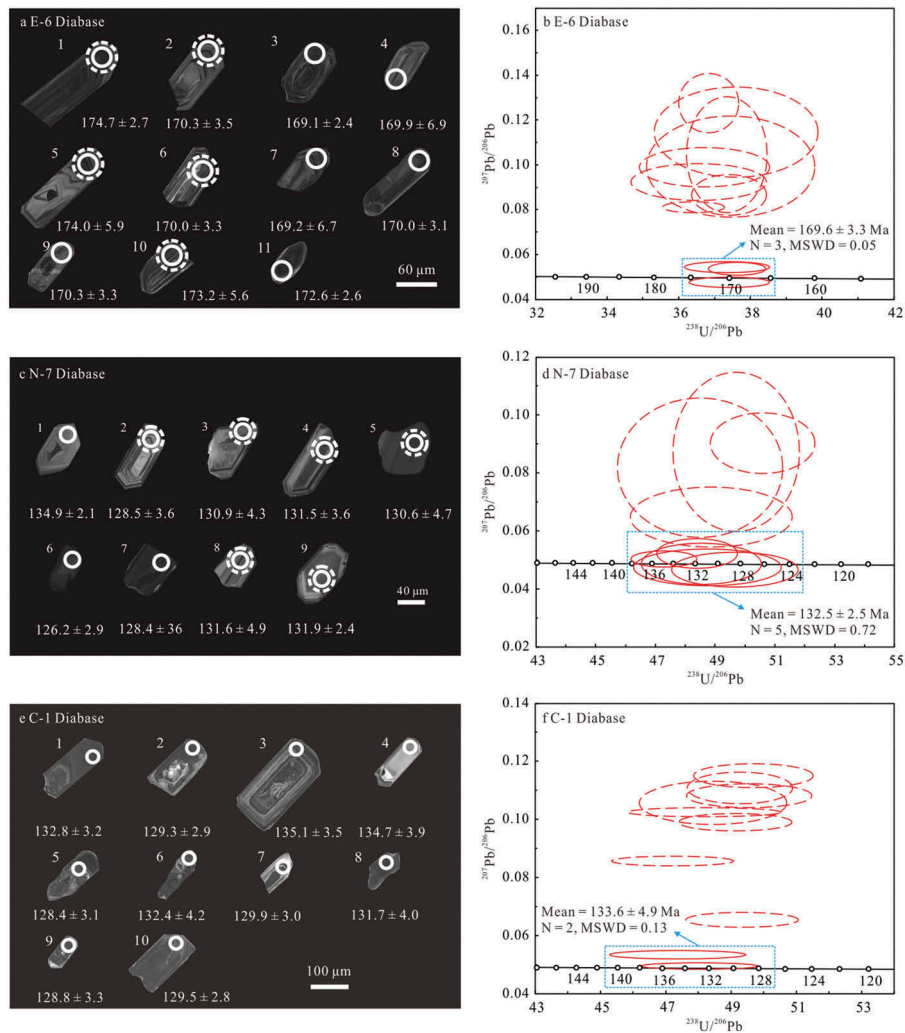


Figure 4. Cathodoluminescence images (a, c, e) and tera-Wasserburg concordia diagrams for U–Pb isotope compositions (b, d, f) of the analysed zircons for the Yilashan diabbases.

50.55 wt.% and CaO from 0.04 to 0.24 wt.%. Three harzburgite samples with MgO contents of 43.23 to 45.36 wt.% are consistent with the corresponding values of typical harzburgite (39.6–48.4 wt.%; Pearce *et al.* 1984). In addition, Mg# [$\text{Mg}^\# = \text{Mg}/(\text{Mg} + \text{Fe}^{\text{total}})$] values of these peridotites vary from 89.5 to 93.4.

The Yilashan peridotites display very low abundances of TREEs (total rare earth elements) ranging from 0.15 to 0.61 ppm. These rocks show approximately U-shaped REE distribution patterns (Figure 5(a)), with $(\text{La}/\text{Yb})_N$ ratios ranging from 1.04 to 11.68, $(\text{La}/\text{Sm})_N$ from 1.37 to 7.59 and $(\text{Gd}/\text{Yb})_N$ from 0.86 to 1.67. The variable Eu anomalies ($\delta\text{Eu} = 0.38\text{--}2.10$, Figure 5(a)) likely indicate the accumulation and fractionation of plagioclases during magma evolution. On the primitive mantle-normalized trace element spidergram (Figure 5(b)), these peridotites are extremely depleted relative to the primitive mantle as a whole and exhibit selective enrichment in large ion lithophile elements (LILEs; e.g.

Ba, U, Pb, and Sr) and depletion in HFSEs. Note that some samples with enrichment of Ta, Hf, and Ti may have resulted from melt–rock interaction. On the plot of Nb/Ta versus Zr/Hf (Figure 6), the Yilashan harzburgites fall into and around the area of the Tonga peridotite rather than abyssal peridotite. Combined with the lower TREE concentration than that of abyssal peridotite (Niu 2004) shown in Figure 5(a), these signatures suggest that the Yilashan harzburgites may not belong to the abyssal peridotites.

5.2.2 Mafic rocks

Twenty-nine mafic rock samples were analysed, and the whole-rock geochemical compositions are shown in Supplementary Table 2. To discuss the geochemical characteristics of these mafic rocks, we also incorporated the geochemical data on mafic rocks from the adjacent Dongqiao (Ye *et al.* 2004; Liu *et al.* 2016), Amdo (Chen *et al.* 2015), Lanong (Xu *et al.* 2010),

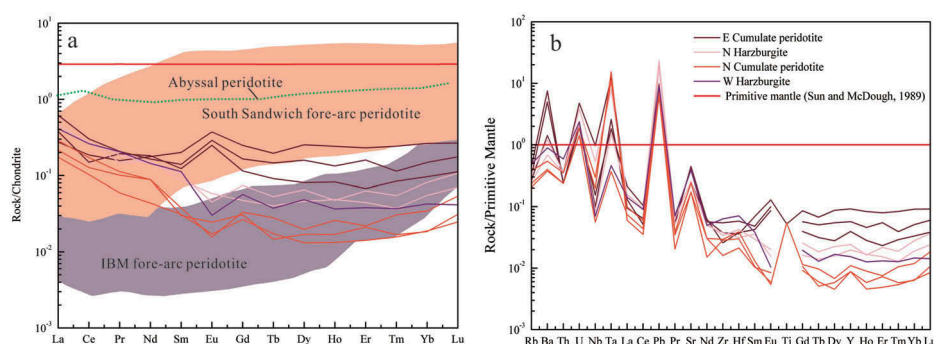


Figure 5. Chondrite-normalized REE (a) and primitive mantle-normalized trace element (b) diagrams for the Yilashan ultramafic rocks. The chondrite and primitive mantle normalization data are from Sun and McDonough (1989). The data for the IBM (Izu-Bonin-Mariana) fore-arc peridotite and South Sandwich fore-arc peridotite are from Parkinson and Pearce (1998) and Pearce *et al.* (2000), respectively.

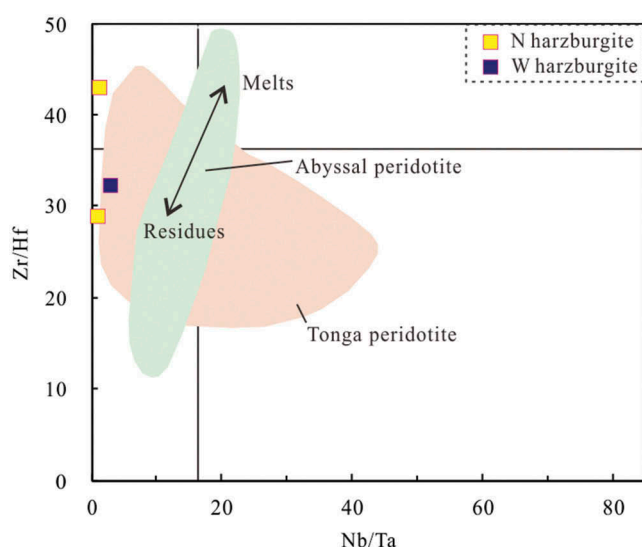


Figure 6. Plot of Nb/Ta versus Zr/Hf (after Kong *et al.* 2012) of the Yilashan ultramafic rocks. Fields for abyssal and Tonga peridotites are from Niu (2004) and Falloon *et al.* (2006), and straight lines delineate chondritic values of Zr/Hf and Nb/Ta.

Pungco (Wang *et al.* 2017), Pungcobei (Huang *et al.* 2015b) and Namco (Zhong *et al.* 2015) ophiolites (Figure 1(b)).

The Yilashan diabase and basalt samples display variable major element contents that have SiO₂ values ranging from 51.78 to 62.89 wt.%, TiO₂ from 0.59 to 1.22 wt.%, Al₂O₃ from 12.87 to 16.42 wt.%, Fe₂O₃T from 6.43 to 9.49 wt.%, MgO from 2.29 to 13.29 wt.% and P₂O₅ from 0.13 to 0.33. Mg[#] values vary widely from 44.60 to 78.38. Some samples have high SiO₂ contents >54.00 wt.% that are likely mainly due to the occurrence of quartz grains (Figure 3(c and d)). These rocks mostly plot in the subalkaline basalt zone on the Nb/Y versus Zr/TiO₂ diagram (Figure 7(a)) and in the calc-alkaline field on the SiO₂ versus FeOT/MgO diagram (Figure 7(b)).

The Yilashan diabase and basalt samples have high amounts of TREEs ranging from 82.50 to 159.10 ppm with an average of 104.67 ppm (Supplementary Table 2). These samples display parallel REE distribution patterns that are enriched in LREEs (Figure 8(a)) with (La/Yb)_N ratios varying from 6.86 to 12.21, (La/Sm)_N from 2.83 to 4.45 and (Gd/Yb)_N from 1.51 to 2.30. Their negative Eu anomalies ($\delta\text{Eu} = 0.71\text{--}0.90$, Figure 8(a)) likely indicate a low level of plagioclase fractionation during magma differentiation. On the N-MORB-normalized trace element spidergram (Figure 8(b)), they feature enrichment in LILEs (e.g. Rb, U, and Sr) but depletion in HFSEs (e.g. Ta, Nb, and Ti). As a whole, the normalized trace element distribution patterns of these rocks show arc volcanic rock characteristics that are different from those of fore-arc basalts (FAB) from the Marianas (Reagan *et al.* 2010) and back-arc basin basalts (BABB) from Central Lau (Tian *et al.* 2008) and Okinawa (Shinjo *et al.* 1999) (Figure 8(a and b)), suggesting an arc-related tectonic setting.

The Yilashan gabbro samples have a broad range of major element contents with SiO₂ from 42.60 to 51.09 wt.%, TiO₂ from 0.03 to 0.15 wt.%, Al₂O₃ from 14.20 to 24.14 wt.%, Fe₂O₃T from 2.67 to 5.62 wt.% and MgO from 8.05 to 23.12 wt.%. Mg[#] values are high ranging from 81.72 to 93.22. They exhibit low concentrations of TREEs ranging from 2.07 to 5.17 ppm with an average of 2.95 ppm (Supplementary Table 2). These rocks display similar REE distribution patterns that are depleted in LREEs (Figure 8(c)) with (La/Yb)_N ratios varying from 0.35 to 1.96, (La/Sm)_N from 0.41 to 1.42 and (Gd/Yb)_N from 11.03 to 1.47. The obviously positive Eu anomalies ($\delta\text{Eu} = 1.24\text{--}2.33$, Figure 8(c)) likely reflect plagioclase accumulation during magma differentiation. On the N-MORB-normalized trace element spidergram (Figure 8(d)), the gabbros exhibit variable enrichment in LILEs (e.g. Rb, Ba, U, and Sr) but depletion in HFSEs (e.g.

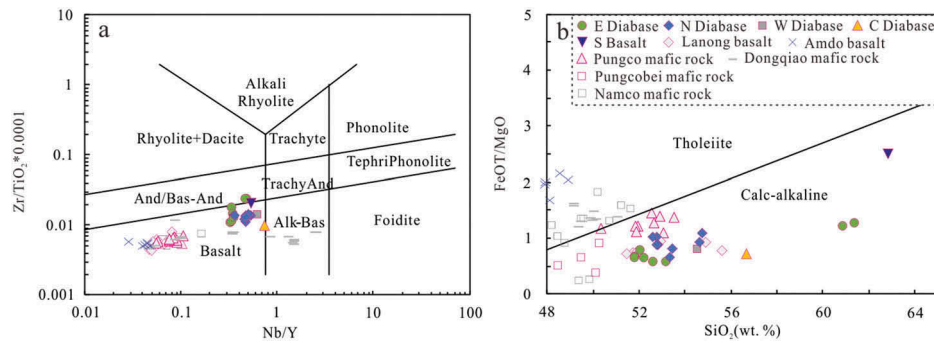


Figure 7. Plots of (a) Nb/Y versus Zr/TiO₂ (after Winchester and Floyd 1977) and (b) SiO₂ versus FeOT/MgO (after Miyashiro 1974) of the Yilashan diabases and basalt. The mafic rocks data from the Lanong, Pungco, Pungcobei, Namco and Amdo ophiolites as shown in Figures 7, 8, 10 and 11 are from Xu *et al.* (2010), Wang *et al.* (2017), Huang *et al.* (2015b), Zhong *et al.* (2015) and Chen *et al.* (2015), respectively. The mafic rocks data for the Dongqiao ophiolite as shown in Figures 7, 8, 10, and 11 are from Ye *et al.* (2004) and Liu *et al.* (2016).

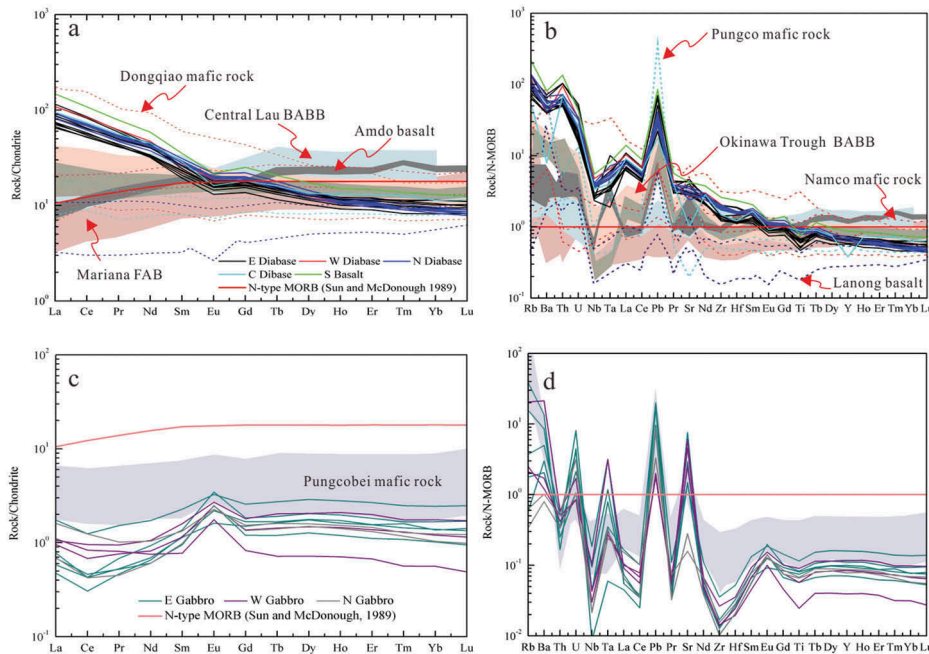


Figure 8. Chondrite-normalized REE (a) and N-MORB-normalized trace element (b) diagrams for the Yilashan mafic rocks. The chondrite and N-MORB normalization data are from Sun and McDonough (1989). The data for the Central Lau BABB (back-arc basin basalt), Okinawa Trough BABB and Mariana FAB (fore-arc basalt) are from Tian *et al.* (2008), Shinjo *et al.* (1999) and Reagan *et al.* (2010), respectively.

Nb, Zr, and Ti). The normalized trace element distribution patterns of these samples are clearly lower than those of N-MORB and the Yilashan diabase and basalt samples (Figure 8). Overall, the high SiO₂ (mostly >45 wt.%) and Mg[#] values (81.72–93.22), together with the extremely low concentrations of HFSEs and positive Eu anomalies (Figure 8(c and d)), reflect that the gabbro samples belong to mafic cumulates. They do not represent liquid compositions that originated from a cooling magma source from which the residual liquid fraction was extracted (Miller *et al.* 2003).

5.3. Sr–Nd–Hf isotopes

Initial Sr–Nd isotopic data were calculated relative to the zircon U–Pb age of 169.6 Ma (E-6) for samples E-8 and E-14. Their (⁸⁷Sr/⁸⁶Sr)_i and (¹⁴³Nd/¹⁴⁴Nd)_i ratios range from 0.705734 to 0.708832 and from 0.512733 to 0.512930, respectively, with ε_{Nd}(t) values varying from +6.1 to +10.0 (Supplementary Table 2). Similarly, sample N-4 has (⁸⁷Sr/⁸⁶Sr)_i, (¹⁴³Nd/¹⁴⁴Nd)_i and ε_{Nd}(t = 132.5 Ma) values of 0.708474, 0.512856, and +7.6, respectively. Note that the western mafic–ultramafic

complex where the N, C, and W samples were collected is in fault contact with the eastern mafic–ultramafic complex where the E samples were collected (Figure 1(c)). This feature, along with the similar zircon U–Pb ages (~133 Ma) obtained from the N, and C diabases (Figure 4(d and f)) and the similar geochemical compositions of the N, C and W samples (Figure 8), indicate that the W samples probably have a formation age similar to these N and C samples. Therefore, $(^{87}\text{Sr}/^{86}\text{Sr})_i$ and $(^{143}\text{Nd}/^{144}\text{Nd})_i$ ratios of the sample W-2 are 0.705389 and 0.512782, respectively, with ϵ_{Nd} ($t = 132.5 \text{ Ma}$) value of +6.1.

Five *in situ* Lu–Hf spot analyses obtained on the dated zircon grains of sample E-6 have initial $^{176}\text{Hf}/^{177}\text{Hf}$ and ϵ_{Hf} ($t = 169.6 \text{ Ma}$) values ranging from 0.282200 to 0.282335 and –16.5 to –11.7, respectively (Supplementary Table 3). The single-stage model ages (T_{DM1}) and two-stage model ages (T_{DM2}) vary from 1.32 to 1.51 Ga and 1.95 to 2.25 Ga, respectively (Supplementary Table 3). Similarly, five *in situ* Lu–Hf spot analyses conducted on the dated zircon grains of sample N-7 display initial $^{176}\text{Hf}/^{177}\text{Hf}$ and ϵ_{Hf} ($t = 132.5 \text{ Ma}$) values ranging from 0.282306 to 0.282679 and –13.6 to –0.4, respectively (Supplementary Table 3). The single-stage model ages (T_{DM1}) and two-stage model ages (T_{DM2}) vary from 0.83 to 1.34 Ga and 1.21 to 2.04 Ga, respectively (Supplementary Table 3).

6. Discussion

6.1. Formation age of the Yilashan mafic and ultramafic rocks and its significance

Two distinct formation ages for gabbro have been reported for the Yilashan mafic–ultramafic complex. Huang *et al.* (2013) reported a zircon LA-ICP-MS U–Pb age of $183.7 \pm 1 \text{ Ma}$ for gabbro, indicating that the Yilashan mafic–ultramafic complex was likely developed in the Early Jurassic. Zhang *et al.* (2014a) proposed an ^{40}Ar – ^{39}Ar age of $114 \pm 2 \text{ Ma}$ on plagioclase from gabbro, implying the occurrence of magmatism in the Early Cretaceous. In this article, three new zircon U–Pb ages of diabase are presented (Supplementary Table 1). An older zircon U–Pb age ($169.6 \pm 3.3 \text{ Ma}$) from sample E-6 is relatively close to the age ($183.7 \pm 1 \text{ Ma}$) of gabbro given by Huang *et al.* (2013), whereas two younger zircon U–Pb ages of samples N-7 ($132.5 \pm 2.5 \text{ Ma}$) and C-1 ($133.6 \pm 4.9 \text{ Ma}$) are closer to the age ($114 \pm 2 \text{ Ma}$) of gabbro reported by Zhang *et al.* (2014a). Note that the diabase samples in this article have similar geochemical signatures (Figure 8(a and b)), which indicates that they probably originated from similar magma sources. The different zircon U–Pb ages, at ~36 Ma intervals, likely indicate that several magmatic intrusions occurred (~169

and ~133 Ma, respectively). Thus, it can be concluded that the Yilashan mafic and ultramafic rocks developed during the Jurassic–Early Cretaceous and likely represent two major igneous events that occurred at 183–169 Ma and 133–114 Ma, respectively.

Isotopic and stratigraphic chronological studies show that the formation ages of the central BNSZ ophiolites are basically clustered in the Jurassic with zircon U–Pb ages ranging from 189 to 148 Ma (Table 1; e.g. Zhu 2004; Sun *et al.* 2011; Zhong *et al.* 2015; Chen *et al.* 2015; Wang *et al.* 2016). Zircon U–Pb ages of Jurassic ophiolites in this region can be further divided into two periods including 178–189 Ma (Amdo, Dongqiao, Pungcobei, Namco and Yunzhug; Zhu 2004; Xia *et al.* 2008; Zhong *et al.* 2015; Huang *et al.* 2015b; Wang *et al.* 2016) and 148–159 Ma (Pungco, Lanong, and Namco; Zhong *et al.* 2015, 2017; Wang *et al.* 2017). It is unusual that ophiolites with Middle Jurassic zircon U–Pb ages are poorly reported. Note that high-Mg andesites in Daruco (Figure 1(b)) yielded zircon U–Pb ages of ~164–162 Ma and occur directly with peridotites (Zeng *et al.* 2016). Zeng *et al.* (2016) argued that these high-Mg andesites belong to the Daruco ophiolite and that the ophiolite was likely generated in the Middle Jurassic. The zircon U–Pb age of $183.7 \pm 1 \text{ Ma}$ of the Yilashan gabbro reported by Huang *et al.* (2013) is consistent with the Early Jurassic formation ages of the ophiolites in the study area. In this article, our older zircon U–Pb age of $169.6 \pm 3.3 \text{ Ma}$ for the Yilashan diabase is younger than the Early Jurassic ophiolites discussed above but resembles the age of the Daruco high-Mg andesites. On the other hand, some Early Cretaceous ophiolitic massifs have been identified in Pungco (basalt, $120 \pm 1.4 \text{ Ma}$; Chen *et al.* 2006), Lanong (gabbro, 128 Ma; Chen *et al.* 2006) and Yunzhug (diabase and basalt at 114–133 Ma and 139 Ma, respectively; Zhu 2004). Our two new ages of $132.5 \pm 2.5 \text{ Ma}$ and $133.6 \pm 4.9 \text{ Ma}$ in this article along with the ^{40}Ar – ^{39}Ar age of $114 \pm 2 \text{ Ma}$ of the Yilashan gabbro reported by Zhang *et al.* (2014a) are consistent with the Early Cretaceous formation ages of these ophiolites. The similar formation ages presented here suggest that the Yilashan mafic–ultramafic complex and the ophiolites listed above likely have some genetic relationships.

6.2. Fractional crystallization and crustal assimilation

The concentrations of Cr and Ni of the Yilashan diabase and basalt samples range widely from 35.2 to 902 ppm and from 27.4 to 278 ppm, respectively (Supplementary Table 2). These values imply that the rocks are variably differentiated compared with those of primitive basaltic magma (Cr = 300–500 ppm, Ni = 300–400 ppm; Frey

et al. 1978). Their slight negative Eu anomalies (Figure 8 (a)) further indicate that crystallization differentiation plays an important role in magma evolution. However, their positive correlations between La and La/Sm (Figure 9(a)), along with the arc-like normalized trace element patterns (Figure 8(a and b)), suggest that the generation of these rocks involved with partial melting and source heterogeneity rather than a simple fractional crystallization.

The selective enrichment in LREEs and depletion in Nb, Ta, Ti, Zr, and Hf of the Yilashan mafic rocks shown in Figure 8 may argue for the involvement of crustal components, either crustal contamination en route or in source regions (Zhao and Zhou 2007). The high Th/La (0.33–0.48, with an average of 0.39) and Th/Ce (0.17–0.25, with an average of 0.20) ratios of the diabase and basalt samples also reflect the possible influence of crustal materials in their petrogenesis (Sun and McDonough 1989; Taylor and McLennan 1995; Plank 2005, 2014). Furthermore, the occurrences of quartz xenoliths and interstitial grains in the diabase (Figure 3(e)) and basalt samples (Figure 3(f)) and the development of granophyre and quartz diorite porphyry in the Yilashan mafic–ultramafic complex (unpublished, this article), further argue for the likely crustal contamination during magmatic evolution. La and Th are enriched in upper continental crust (UCC), whereas Th is generally depleted in lower continental crust (LCC) (Barth *et al.* 2000). The diabase and basalt samples are clearly enriched in Th, which may reflect the addition of UCC materials. On the diagram of $(\text{Nb/La})_{\text{PM}}$ ('PM' denotes normalization to primitive mantle composition) versus $(\text{Zr/Nd})_{\text{PM}}$ (Figure 9(b)), the diabase and basalt samples plot in a field nearer to the upper crust (UC) than to the low crust (LC), further arguing for the influences of UC components. In addition, the Yilashan mafic rocks exhibit variable $(^{87}\text{Sr}/^{86}\text{Sr})_i$ values (0.705389–0.708832) and clearly positive $\epsilon_{\text{Nd}}(t)$ values

(+6.1 to +10.0), and they plot far away from the GLOSS (global oceanic sediment) and LCC fields on the $(^{87}\text{Sr}/^{86}\text{Sr})_i$ versus $\epsilon_{\text{Nd}}(t)$ diagram (Figure 10(a)). Therefore, the signatures presented here probably indicate limited input of crustal components during magmatic evolution, and the most likely candidate for the crustal materials may be the upper crust. Cr (35.2–902 ppm, with an average of 411 ppm) and Ni (27.4–278 ppm, with an average of 161 ppm) values of the diabase and basalt samples also argue against extensive crustal assimilation.

6.3. Nature of magma sources

Peridotites are generally considered to be the residuum after partial melting of primary mantle (Coleman 1977; Hawkins 2003). In the process of magma differentiation, residua are depleted in Nb, Ta, Zr, and Hf with Nb/Ta and Zr/Hf ratios generally lower than those of chondrites (17.57 and 36.3, respectively; Falloon *et al.* 2006). Two samples of the Yilashan harzburgites have lower ratios of Nb/Ta (0.96–2.66) and Zr/Hf (29.0–32.3), further showing a feature of mantle residuum (Figure 6). Note that one sample with higher Zr/Hf value (43.1) compared with chondrite may be caused by rock-melt interaction (Falloon *et al.* 2006) (Figure 6). Meanwhile, the enrichment of Ta, Hf, and Ti in some peridotite samples (Figure 5(b)) also argues for likely rock-melt interaction. Moreover, the Yilashan peridotites have very low trace element concentrations with strong enrichment in LREEs and LILEs (Figure 5), which is generally associated with partial melting of a depleted mantle source modified by LREE-enriched fluids and/or melts that originated from the subducting slab or sediments (Niu 2004; Paulick *et al.* 2006; Dai *et al.* 2011). Considering that the addition of subducted sediments in the magma sources and crustal contamination in a later

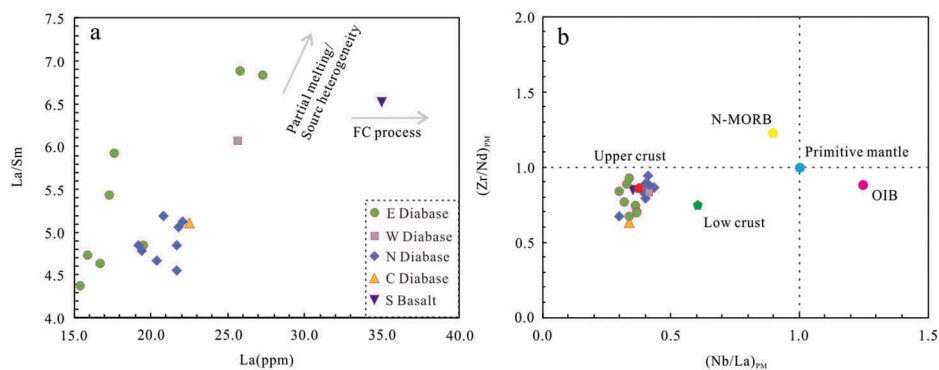


Figure 9. Plots of (a) La versus La/Sm and (b) $(\text{Nb/La})_{\text{PM}}$ versus $(\text{Zr/Nd})_{\text{PM}}$ for the Yilashan diabases and basalt. Values for the lower and upper crust are from Wedepohl (1995), and values of primitive mantle, N-MORB (normal mid-ocean ridge basalt) and OIB (ocean island basalt) are from Sun and McDonough (1989).

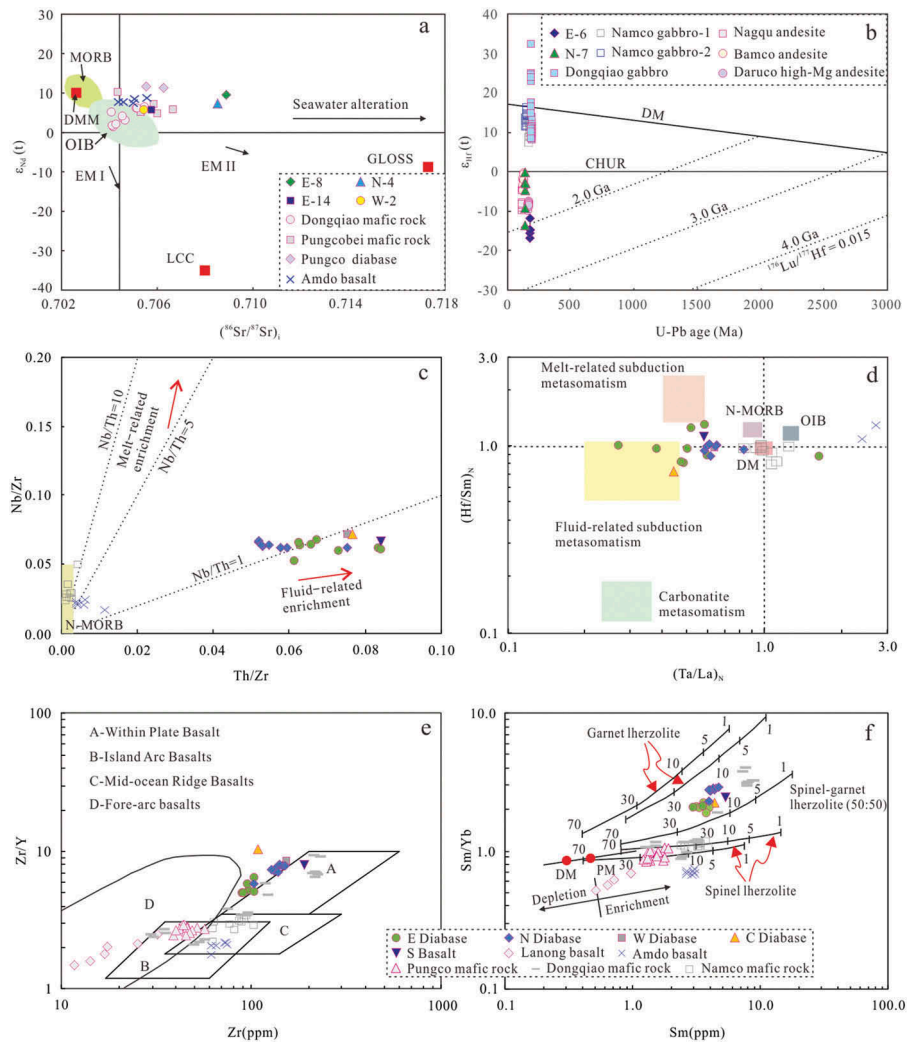


Figure 10. Plots of (a) $(^{87}\text{Sr}/^{86}\text{Sr})_i$ versus $\epsilon_{\text{Nd}}(t)$ (after Meng *et al.* 2015, and references therein), (b) zircon $\epsilon_{\text{Hf}}(t)$ versus zircon U–Pb age, (c) Th/Zr versus Nb/Zr (after Kepezhinskas *et al.* 1997), (d) $(\text{Ta}/\text{La})_N$ versus $(\text{Hf}/\text{Sm})_N$ (after LaFlèche *et al.* 1998), (e) Zr versus Zr/Y (after Pearce and Norry 1979) and (f) Sm versus Sm/Yb (after Zhao and Zhou 2007, and references therein) for the Yilashan mafic rocks. The numbers on the curves indicate the degree of partial melting in (f). DMM: depleted MORB mantle; EM: enriched mantle; MORB: mid-ocean ridge basalt; LCC: lower continental crust; GLOSS: global oceanic sediment; CHUR: chondritic uniform reservoir; OIB: ocean island basalt; N-MORB: normal mid-ocean ridge basalt; DM: depleted mantle; PM: primitive mantle.

stage may be limited (Figure 10(a)) and that the magma sources of the diabase and basalt samples were mainly affected by subducted fluids rather than melts (discussed later), the mantle source of the Yilashan peridotites would be mainly modified by the fluids derived from the subducting slab. Some peridotites showing clear magnesite mineralization (unpublished, this article) are consistent with this inference. In addition, although boninites have been identified in the diabasic dikes of the Pungco ophiolite (Pearce and Deng 1988) in the study area (Figure 1(b)), the Yilashan mafic and ultramafic rocks likely formed in a continental arc setting (see below), which rules out the possibility that the boninitic magmas reacted with the Yilashan peridotites.

Negative zircon $\epsilon_{\text{Hf}}(t)$ values and older Hf model ages of the samples E-6 ($\epsilon_{\text{Hf}}(t)$ values of -16.5 to -11.7 , $T_{\text{DM}1}$ of 1.32 to 1.51 Ga and $T_{\text{DM}2}$ of 1.95 to 2.25 Ga) and N-7 ($\epsilon_{\text{Hf}}(t)$ values of -13.6 to -0.4 , $T_{\text{DM}1}$ of 0.83 to 1.34 Ga and $T_{\text{DM}2}$ of 1.21 to 2.04 Ga) (Supplementary Table 3; Figure 10(b)) suggest that ancient crust or lithospheric mantle was involved in the generation of the Yilashan diabase and basalt samples. However, significant crustal contamination is precluded. Again, previous studies based on zircon Lu–Hf isotopes of igneous rocks and whole-rock Nd isotopes of clastic sedimentary rocks reflect that the northern Lhasa terrane is characterized by younger and juvenile crust (Zhu *et al.* 2009, 2011, 2013, 2016).

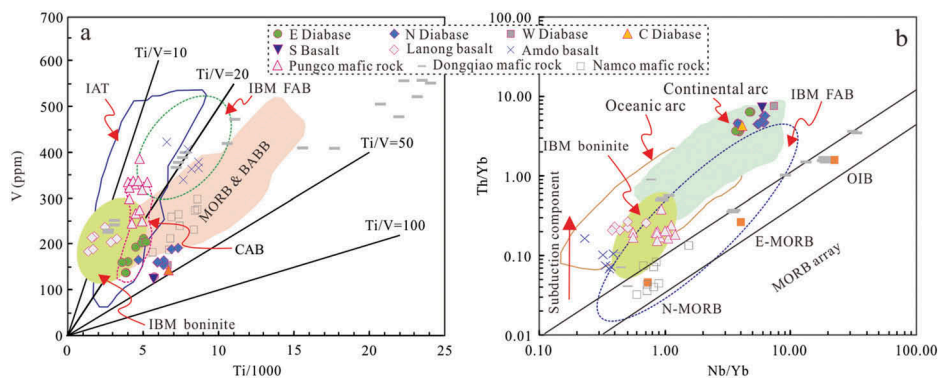


Figure 11. Plots of (a) Ti versus V (after Shervais 1982) and (b) Nb/Yb versus Th/Yb (after Pearce and Peate 1995) for the Yilashan diabases and basalt. MORB: mid-ocean ridge basalt; IAT: island-arc tholeiite; CAB: calc-alkaline basalt; BABB: back-arc basin basalt; FAB: fore-arc basalt; OIB: ocean island basalt; N-MORB: normal mid-ocean ridge basalt; E-MORB: enriched mid-ocean ridge basalt; IBM: Izu-Bonin-Mariana.

These signatures, in combination with the identification of ancient lithospheric mantle materials in the magma sources of the adjacent Middle Jurassic high-Mg andesites in Daruco ($\epsilon_{\text{Hf}}(t)$ values of -9.9 to -7.4 and $T_{\text{DM}2}$ of 1.7 to 1.8 Ga; Zeng *et al.* 2016), Early Cretaceous andesites in Nagqu ($\epsilon_{\text{Hf}}(t)$ values of -9.9 to -4.7 , $T_{\text{DM}1}$ of 0.94 to 1.15 Ga and $T_{\text{DM}2}$ of 1.36 to 1.68 Ga; Huang *et al.* 2012) and Bamco ($\epsilon_{\text{Hf}}(t)$ values of -4.6 to -0.3 , $T_{\text{DM}1}$ of 0.80–0.97 Ga and $T_{\text{DM}2}$ of 1.20 to 1.47 Ga; Chen *et al.* 2010) and Early Cretaceous granites in Daruco ($\epsilon_{\text{Hf}}(t)$ values of -5.5 to -2.6 and $T_{\text{DM}2}$ of 1.34 to 1.52 Ga; Tang *et al.* 2015) (Figures 1(b) and 10(b)), are indicative of the probable influence of ancient lithospheric mantle components in the study area. In addition, $^{187}\text{Os}/^{188}\text{Os}$ ratios of harzburgites and dunites from the Dongqiao ophiolite and Yilashan mafic–ultramafic complex range from 0.1174 to 0.1316 with Re-Depletion (TRD) model ages up to 1.43 Ga that further argue for a Mesoproterozoic lithospheric mantle source in the study area, which had experienced mantle re-fertilization and then was metasomatized by percolation of melts and/or fluids (Huang *et al.* 2015a).

The Yilashan diabase and basalt samples exhibit enrichment in LILEs and LREEs but depletion in HFSEs (e.g. Nb, Ta, and Ti) (Figure 8(a and b)). They have ratios of Nb/La (0.31–0.45) < 1 , Zr/Nb (13.78–18.97) > 5.8 (OIB) and $(\text{Th}/\text{Nb})_{\text{PM}}$ (6.45–11.53) > 1 (which are distinct from that of asthenosphere-derived basalts at less than 1; Saunders *et al.* 1992). These signatures, combined with their low TiO_2 contents (0.59–1.22 wt.%), argue for a metasomatized lithospheric mantle source instead of an asthenospheric mantle source (Lightfoot *et al.* 1993; Ewart *et al.* 1998; Wang *et al.* 2005). Moreover, the variable zircon $\epsilon_{\text{Hf}}(t)$ values of samples E-6 (-16.5 to -11.7) and N-7 (-13.6 to -0.4) suggest hybrid magmas in the source region. Th/Zr and Nb/Zr ratios can be used

to constrain the influences of subduction-related melts and/or fluids in the magma source (Kepezhinskis *et al.* 1997). On the Th/Zr versus Nb/Zr diagram (Figure 10(c)), the diabase and basalt samples have high Th/Zr relative to Nb/Zr and plot along the trajectory of fluid-related enrichment. Similarly, these samples display a wide range of $(\text{Ta}/\text{La})_{\text{N}}$ relative to $(\text{Hf}/\text{Sm})_{\text{N}}$ that basically falls along the trajectory between OIB and arc materials metasomatized by subducted fluids in the plot of $(\text{Ta}/\text{La})_{\text{N}}$ versus $(\text{Hf}/\text{Sm})_{\text{N}}$ (Figure 10(d)). It can be concluded that the magma source of the diabase and basalt samples was mainly modified by subducted fluids instead of slab-related melts. Note that the dunites of the Yilashan mafic–ultramafic complex likely originated from a weakly depleted asthenospheric mantle source based on Os-isotopes of Cr-spinel (Huang *et al.* 2013). Again, the Yilashan diabase and basalt samples have relatively high Zr/Y relative to Zr, which shows some characteristics of within-plate basalts (WPB) rather than those of island arc basalts (IAB) and MORB on the plot of Zr versus Zr/Y (Figure 10(e)). Combined with the positive $\epsilon_{\text{Nd}}(t)$ values ($+6.1$ to $+10.0$) of the Yilashan mafic rocks, these signatures indicate that the Yilashan mafic rock samples likely originated from an ancient lithospheric mantle source that interacted with magmas due to asthenospheric upwelling. Nd–Hf isotopic decoupling of the Yilashan mafic rock samples was probably related to the fact that different isotopic systems have different rates of equilibration in the magma mixing process such that the whole-rock Sr–Nd isotopes can much more quickly homogenize in this process, whereas the zircon Lu–Hf isotopes do not easily reach equilibrium (e.g. Leshner 1990; Scherer *et al.* 2000; Griffin *et al.* 2002; Hu *et al.* 2005). Therefore, the positive $\epsilon_{\text{Nd}}(t)$ values ($+6.1$ to $+10.0$) of the Yilashan mafic rocks probably indicate a rapid rate of equilibration during

magma mixing of two end-members (ancient lithospheric mantle source and weakly depleted asthenospheric mantle source), whereas the variable negative $\epsilon_{\text{Hf}}(t)$ values of -0.4 to -13.6 and -11.7 to -16.3 have preserved details of the assembly of the different magmas (Griffin *et al.* 2002).

REEs are widely used to identify magma genesis and degrees of partial melting of a mantle source (Zhao and Zhou 2007). Most of the Yilashan diabase and basalt samples have Ce/Y ratios (1.75–4.27, with an average of 2.34) less than 3, which reflect a stable spinel-garnet mantle field at 60–80 km deep (McKenzie and Bickle 1988), consistent with the observation that Cr-spinels are enriched in the Yilashan peridotites (Figure 3(a and b)). On the plot of Sm versus Sm/Yb (Figure 10(f)), the diabase and basalt samples display relatively high Sm/Yb ratios that fall in the field between the melting curves of spinel-garnet lherzolite and garnet lherzolite but are closer to the former, implying that these rocks probably formed by ~10–25% partial melting of a garnet + minor spinel lherzolite mantle source.

6.4. Tectonic setting

The Yilashan peridotites exhibit low trace element concentrations with approximately U-shaped REE patterns, selective enrichment in LILEs and depletion of Nb (Figure 5). These signatures, combined with the conclusion that Yilashan harzburgites are distinct from abyssal peridotite as shown in Figures 5(a) and 6, indicate that the Yilashan peridotites developed in a SSZ setting.

The Yilashan diabase and basalt samples display geochemical features of arc volcanic rocks with enrichment in LREEs and LILEs and depletion in HFSEs (Figure 8(a and b)), suggesting an arc setting. Note that these rocks plot in and around the WPB field on the Zr versus Zr/Y diagram (Figure 10(e)), which may be associated with the influences of asthenospheric upwelling in the magma source. Several tectonic discrimination diagrams are used to determine the tectonic setting of the Yilashan diabase and basalt samples in the following. These samples fall in and around the overlapping fields of IAT (island arc tholeiite) and CAB (calc-alkaline basalt) on the Ti versus V diagram (Figure 11(a)). These signatures, along with these rocks plotting in the continental arc zone on the Nb/Yb versus Th/Yb diagram (Figure 11(b)), suggest that they likely formed in a continental margin arc setting. Further support is provided by these samples showing high Th/Yb values that plot in and around the active continental margin field on the Ta/Yb versus Th/Yb diagram (not shown; Pearce 1983; Xiao *et al.* 2004). Although three new zircon U–Pb ages ranging from Middle

Jurassic to Early Cretaceous are obtained from different diabase samples in distinct locations (Figure 1(c)), the similar geochemical compositions of these samples (Figure 8(a and b)) indicate that the Yilashan mafic and ultramafic rocks likely developed in a single continental arc setting with similar magma sources during the Jurassic–Early Cretaceous.

6.5. Comparison with Jurassic–Early Cretaceous ophiolites in the central BNSZ

The Dongqiao, Amdo, Pungco, Pungcobei, Lanong, and Namco ophiolites occurring in the study area (Figure 1(b)) are briefly compared with the Yilashan mafic rocks to better understand the petrogenesis and hence to evaluate the regional geological setting.

The Dongqiao and Amdo ophiolites to the north are located at the southern margin of the Qiangtang terrane (Figure 1(b)). The Dongqiao ophiolite comprises IAB, MORB (N-MORB and E-MORB) and OIB-like mafic rocks with scattered points shown partly in Figures 7, 8, 10 and 11 (Ye *et al.* 2004; Liu *et al.* 2016; Wang *et al.* 2016). These mafic rocks exhibit relatively low $(^{87}\text{Sr}/^{86}\text{Sr})_t$ and $\epsilon_{\text{Nd}}(t)$ values with positive zircon $\epsilon_{\text{Hf}}(t)$ values relative to the Yilashan mafic rock samples (Figure 10(a and b)). Again, these rocks have a wide range of Sm and Sm/Yb values that show diversified magma sources with respect to the Yilashan diabase and basalt samples (Figure 10(f)). The Amdo basalts (Figure 7(a)) display the mixed end-numbers of arc and N-MORB geochemical features and originated from an N-MORB-like depleted mantle source that was composed of spinel lherzolite (Figures 8, 10 and 11). These signatures are distinct from those of the Yilashan mafic rock samples. Recently, studies have proposed that the Dongqiao (181–188 Ma; Xia *et al.* 2008; Liu *et al.* 2016; Wang *et al.* 2016) and Amdo (184–220 Ma; Sun *et al.* 2011; Chen *et al.* 2015; Wang *et al.* 2016) ophiolites were probably produced in an intra-oceanic subduction setting (Chen *et al.* 2015; Wang *et al.* 2016) during the Late Triassic–Early Jurassic as a result of the northward subduction of the BNTO beneath the Qiangtang terrane.

Mafic rocks of the Pungco (Wang *et al.* 2017), Pungcobei (Huang *et al.* 2015b) and Lanong (Xu *et al.* 2010) ophiolites are also shown in Figures 7, 8, 10 and 11. These rocks display $\epsilon_{\text{Nd}}(t)$ values similar to those of the Yilashan mafic rock samples (Figure 10(a)), but have low values of Sm and Sm/Yb that imply a spinel lherzolite mantle source with high partial melting that is different from that of the Yilashan diabase and basalt samples (Figure 10(f)). Furthermore, these rocks have various degrees of fore-arc basalt or boninite geochemical features (Figures 8, 10(e) and 11). Combined with

the nearby Pungco boninites (Pearce and Deng 1988) and the Daruco continental margin high-Mg andesites that are in direct contact with peridotites (Zeng *et al.* 2016), these signatures indicate that a continental fore-arc lithosphere likely formed during the Jurassic–Early Cretaceous (188–120 Ma; Table 1) represented by the Pungco-Lanong (including the Daruco and Pungcobei ophiolites) ophiolitic mélange as a result of the southward subduction of the BNTO beneath the Lhasa terrane (e.g. Wang *et al.* 2017; Zhong *et al.* 2017).

The southernmost Namco ophiolite is located at the southern margin of the northern Lhasa terrane (Figure 1(b)). Mafic rocks of the Namco ophiolite exhibit the mixed end-members of arc and N-MORB geochemical features, and were derived from an N-MORB-like depleted mantle source that was composed of spinel lherzolite (Figures 8, 10 and 11). These features are different from those of the Yilashan mafic rock samples. Zhong *et al.* (2015) proposed that the Namco ophiolite (178–149.7 Ma) formed in a continental back-arc basin during the Jurassic related to the southward subduction of the BNTO beneath the Lhasa terrane.

6.6. Tectonic implications

The BNTO had experienced a series of complex tectonic evolutionary processes with ancient continent break-up, seafloor spreading and consumption and collision of the Lhasa–Qiangtang terranes over geological periods (Zhu *et al.* 2013; Zhang *et al.* 2014b, 2017; Liu *et al.* 2017a, 2017; Zhang and Zhang 2017). It is beyond the scope of this study to discuss the early evolution of the BNTO, and the BNTO probably had already evolved into a wide ocean in the Early Jurassic (Pan *et al.* 2006, 2012; Zhu *et al.* 2013; Zhang *et al.* 2014b; Chen *et al.* 2015; Zhang and Zhang 2017).

A series of Jurassic magmatic rocks is located at the southern margin of the Qiangtang terrane (e.g. Kapp *et al.* 2005; Li *et al.* 2014; Liu *et al.* 2014; Hao *et al.* 2015; Zhang *et al.* 2017) and the Amdo terrane (Guynn *et al.* 2006; Liu *et al.* 2010; Zhu *et al.* 2011). These rocks, along with the occurrence of a Late Triassic–Jurassic accretionary wedge at the southern margin of the Qiangtang terrane (Zeng *et al.* 2015; Liu *et al.* 2017), indicate the northward subduction of the BNTO beneath the Qiangtang–Amdo terranes as early as the Late Triassic. The whole-rock geochemical and zircon Lu–Hf isotopic data of the Yilashan diabase and basalt samples (Supplementary Tables 2 and 3) suggest that these rocks formed by involvement with ancient lithospheric mantle components. The Yilashan mafic–ultramafic complex is located between the Amdo and central Lhasa terranes (Figure 1(c)). Considering that both the

Amdo and central Lhasa terranes have ancient metamorphic crystalline basement (e.g. Zhu *et al.* 2009, 2011, 2013; and references therein), either of them could have been involved in the formation of the Yilashan mafic and ultramafic rocks. However, the Amdo terrane involvement in the generation of the Yilashan mafic and ultramafic rocks can be excluded, as explained in the following discussion. Recently, studies have indicated that the Amdo terrane was an isolated microcontinent in the BNTO during the Permian–Triassic (e.g. Zhu *et al.* 2013; Zhang *et al.* 2014c). This terrane had experienced granitoid magmatism (Guynn *et al.* 2006; Zhu *et al.* 2011) and coeval high-pressure metamorphism (Guynn *et al.* 2006; Shi *et al.* 2012, 2013; Zhang *et al.* 2012, 2014c) in the Early Jurassic, likely as a result of the same event of the northward subduction of the Amdo terrane under the Amdo intra-oceanic back-arc basin (Chen *et al.* 2015) or the Qiangtang terrane (e.g. Zhu *et al.* 2011; Zhang *et al.* 2012, 2014c). During this subduction process, the Amdo terrane was exhumed to mid-crustal levels in the Early Jurassic (~181 Ma) along with obvious metamorphism and granitoid magmatism (Zhang *et al.* 2014c) (Figure 12(a)). Thus, there were probably no proper conditions to generate the Yilashan mafic and ultramafic rocks associated with the Amdo terrane in the Early Middle Jurassic (~183–170 Ma). Furthermore, the zircon $\varepsilon_{\text{Hf}}(t)$ values (–16.5 to –0.4) of the diabase and basalt samples is distinct from those of Mesozoic rocks in the Amdo terrane (–11.1 to +0.6; Zhu *et al.* 2011, and references therein), which possibly implies a more enriched magma source. However, these values lie in the range of zircon $\varepsilon_{\text{Hf}}(t)$ values (–22.0 to +9.6) of Mesozoic–Early Tertiary magmatic rocks in the central Lhasa terrane (Zhu *et al.* 2011, and references therein). In combination with the observation that the central Lhasa terrane used to be an ancient microcontinent and the idea that the initial southward subduction of the BNTO beneath the Lhasa terrane was likely at the Middle Permian (e.g. Pan *et al.* 2006, 2012; Zhu *et al.* 2009, 2011, 2013), the development of the Jurassic–Early Cretaceous Yilashan mafic and ultramafic rocks could have been related to the southward subduction of the BNTO beneath the central Lhasa terrane. Nonetheless, the Yilashan mafic–ultramafic complex is relatively far away from the central Lhasa terrane at present (Figure 1(b)), especially since the northern Lhasa terrane had experienced significant shortening (>50%) from the Late Cretaceous to Palaeogene (Zhu *et al.* 2009, and references therein). Note that some Middle Jurassic–Early Cretaceous magmatic rocks with negative zircon $\varepsilon_{\text{Hf}}(t)$ values and old Hf model ages (Chen *et al.* 2010; Huang *et al.* 2012; Tang *et al.* 2015; Zeng *et al.* 2016) are developed in the study

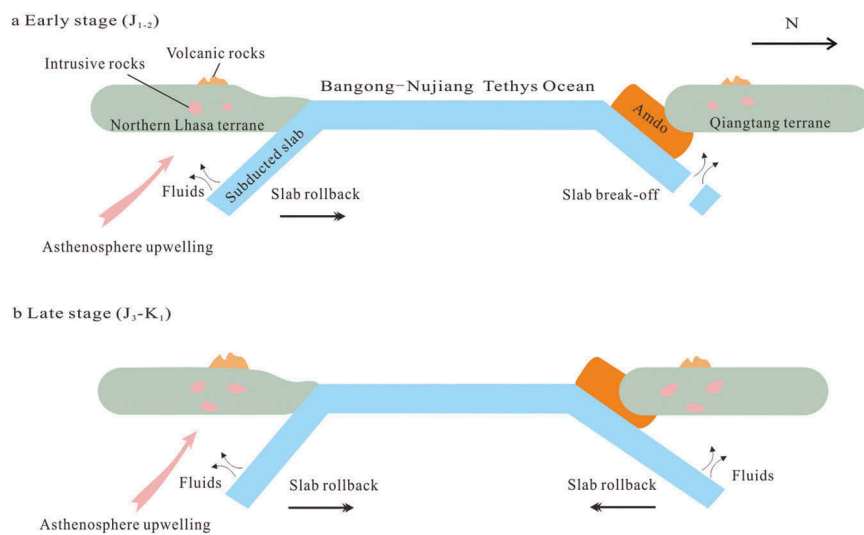


Figure 12. Simplified tectonic evolutionary model for the Yilashan mafic and ultramafic rocks (after Zhang *et al.* 2014c, 2017). Not drawn to scale. The Yilashan mafic and ultramafic rocks formed during the Jurassic–Early Cretaceous in a continental margin arc setting as a result of the southward subduction of the Bangong–Nujiang Tethys Ocean beneath the Lhasa terrane. Please see text for more details.

area, suggesting that an ancient basement likely existed beneath the study area (Liu *et al.* 2016). Huang *et al.* (2015a) further proposed that old mantle domains probably existed in the BNSZ as remnants of ancient sub-continental lithospheric mantle (SCLM). Therefore, the study area is not simply characterized by younger and juvenile crust (Zhu *et al.* 2009, 2011; Zeng *et al.* 2016). The Yilashan mafic and ultramafic rocks likely formed related to the southward subduction of the BNTO beneath the (northern) Lhasa terrane.

It is worth noting that the Dongqiao ophiolite contains Early Jurassic OIB-type basalts (Liu *et al.* 2016). Interbedded OIB-type basalts in Middle Triassic radiolarian cherts (237–228 Ma) of the Nagqu Gajia Formation (T_{2-3g}) (Zhu *et al.* 2006) and Early Cretaceous OIB-type basalts in Duoma (Zhu *et al.* 2006) and Tarenben (Wang *et al.* 2005) have also been identified in the central BNSZ. Zhang *et al.* (2014a) suggested that there were two major plateau eruptive events at 193–173 Ma and 128–104 Ma in the BNTO due to mantle plume upwelling. These signatures imply that mantle plume activity likely had played an important role in the evolution of the central BNSZ during the Mesozoic. Meanwhile, Cr-spinel of the Yilashan dunites shows Os isotopic features similar to those of slightly depleted asthenospheric mantle (Huang *et al.* 2013), indicating the input of materials derived from an asthenospheric mantle plume (Zhao *et al.* 1994) or plume-fed asthenosphere (Hasenclever *et al.* 2005). Therefore, the Yilashan mafic and ultramafic rocks were likely produced by the processes in which an ancient lithospheric mantle wedge was modified mainly by asthenosphere-derived magmas and subducted fluids with two major igneous events at ~183–

170 Ma and ~133–114 Ma as a result of the southward subduction of the BNTO beneath the Lhasa terrane (e.g. Zhu *et al.* 2011; Sui *et al.* 2013) (Figure 12). In addition, much magmatism also occurred in the northern Lhasa terrane during this period (Figure 12; e.g. Kang *et al.* 2008; Zhu *et al.* 2008, Zhu *et al.* 2013, 2016). In particular, the orthopyres from the Pungco area (Figure 1(b)) formed with a zircon U–Pb age of 170 ± 2.4 Ma and a continental arc setting (Yi *et al.* 2017) that is consistent with the early stage (~183–170 Ma) of the Yilashan mafic–ultramafic complex.

Because of the S–N-trending horizontal compressional stress caused by the southward subduction of the BNTO and the northward subduction of the Yarlung Zangbo Neo-Tethys Ocean, the BNTO finally closed with the collision of the Lhasa and Qiangtang (including the Amdo terrane) terranes after the late Early Cretaceous (e.g. Zhu *et al.* 2011, 2016; Sui *et al.* 2013; Fan *et al.* 2015; Liu *et al.* 2017).

7. Conclusions

- (1) Three zircon U–Pb ages of 169.6 ± 3.3 , 132.5 ± 2.5 , and 133.6 ± 4.9 Ma are obtained from diabases. These ages, along with other two ages presented by previous studies, suggest that the Yilashan mafic–ultramafic complex was likely generated in the Jurassic–Early Cretaceous with two major igneous events that occurred at ~183–170 Ma and ~133–114 Ma, respectively;

- (2) The Yilashan mafic and ultramafic rocks formed in a continental arc setting as a result of the southward subduction of the Bangong–Nujiang Tethys Ocean beneath the Lhasa terrane;
- (3) The Yilashan mafic and ultramafic rocks originated from an ancient lithospheric mantle source with the addition of weakly depleted asthenospheric components and subducted fluids along with limited crustal contamination. The diabase and basalt samples were probably derived by ~10–25% partial melting of a garnet + minor spinel lherzolite mantle source.

Acknowledgements

This work was supported by the National Nature Science Foundation of China (grant 41472054 and 41372208); the Open found of the State Key Laboratory of Ore Deposit Geochemistry, Chinese Academy of Sciences (grant 201304); and Tibetan Special Foundation of China Geological Survey (grant 1212011221105). We appreciate Hong-Fei Liu, Zheng-Xin Yin and Yun-Deng Reji for their help in field work and Guo-Qing Zhou, Liang Qi and Zhi-Hui Dai for their analytical assistance.

Disclosure statement

No potential conflict of interest was reported by the authors.

Funding

This work was supported by the China Geological Survey [grant number 1212011221105]; National Natural Science Foundation of China [grant numbers 41372208 and 41472054]; the Open found of the State Key Laboratory of Ore Deposit Geochemistry, Chinese Academy of Sciences [grant number 201304].

ORCID

Yun Zhong  <http://orcid.org/0000-0002-9094-1925>
 Xi-Chong Hu  <http://orcid.org/0000-0002-1409-3960>
 Wei-Liang Liu  <http://orcid.org/0000-0002-7556-6565>
 Xiao Zhang  <http://orcid.org/0000-0002-1214-3936>

References

- Barth, M.G., McDonough, W.F., and Rudnick, R.L., 2000, Tracking the budget of Nb and Ta in the continental crust: *Chemical Geology*, v. 165, no. 3–4, p. 197–213. [10.1016/S0009-2541\(99\)00173-4](https://doi.org/10.1016/S0009-2541(99)00173-4)
- Bau, M., 1991, Rare-earth element mobility during hydrothermal and metamorphic fluid-rock interaction and the significance of the oxidation state of europium: *Chemical Geology*, v. 93, no. 3–4, p. 219–230. doi:[10.1016/0009-2541\(91\)90115-8](https://doi.org/10.1016/0009-2541(91)90115-8)
- Blichert, T.J., and Albarede, F., 1997, The Lu–Hf geochemistry of the chondrites and the evolution of the mantle-crust system: *Earth and Planetary Science Letters*, v. 148, p. 243–258. [10.1016/S0012-821X\(97\)00198-2](https://doi.org/10.1016/S0012-821X(97)00198-2)
- Bureau of Geology and Mineral Resources of Tibet, 1993, *Regional geology of the Tibet*: Beijing, Geology Publishing House. [In Chinese.]
- Chen, L., Zhao, Z.F., and Zheng, Y.F., 2014, Origin of andesitic rocks: Geochemical constraints from Mesozoic volcanics in the Luzong basin, South China: *Lithos*, v. 190–191, p. 220–239. [10.1016/j.lithos.2013.12.011](https://doi.org/10.1016/j.lithos.2013.12.011)
- Chen, S.S., Shi, R.D., Zou, H.B., Huang, Q.S., Liu, D.L., Gong, X.H., Yi, G.D., and Wu, K., 2015, Late Triassic island-arc-back-arc basin development along the Bangong–Nujiang suture zone (central Tibet): Geological, geochemical and chronological evidence from volcanic rocks: *Lithos*, v. 230, p. 30–45. [10.1016/j.lithos.2015.05.009](https://doi.org/10.1016/j.lithos.2015.05.009)
- Chen, Y., Zhu, D.C., Zhao, Z.D., Zhang, L.L., Liu, M., Yu, F., Guan, Q., and Mo, X.X., 2010, Geochronology, geochemistry and petrogenesis of the Bamco andesites from the northern Gangdese, Tibet: *Acta Petrologica Sinica*, v. 26, p. 2193–2206. In Chinese with English abstract.
- Chen, Y.L., Zhang, K.Z., Li, G.Q., Nimaciren, Z., and Chen, G.R., 2005, Discovery of a uniformity between the Upper Triassic Quehala Group and its underlying rock series in the central segment of the Bangong Co–Nujiang junction zone, Tibet, China: *Geological Bulletin of China*, v. 24, p. 621–624. [In Chinese with English abstract.]
- Chen, Y.L., Zhang, K.Z., and Yang, Z.M., 2006, Discovery of a complete ophiolite section in the Jueweng area, Nagqu county, in the central segment of the Bangong Co–Nujiang junction zone: Qinghai–Tibet plateau: *Geological Bulletin of China*, v. 25, no. 6, p. 694–699. [In Chinese with English abstract.]
- Chu, M.F., Chung, S.L., Song, B., Liu, D.Y., O’Reilly, S.Y., Pearson, N.J., Ji, J.Q., and Wen, D.J., 2006, Zircon U–Pb and Hf isotope constraints on the Mesozoic tectonics and crustal evolution of southern Tibet: *Geology*, v. 34, p. 745–748. [10.1130/G22725.1](https://doi.org/10.1130/G22725.1)
- Coleman, R.G., 1977, *Ophiolites: Ancient oceanic lithosphere?*: Berlin, Heidelberg, Springer Verlag.
- Dai, J.G., Wang, C.S., Hébert, R., Santosh, M., Li, Y.L., and Xu, J. Y., 2011, Petrology and geochemistry of peridotites in the Zhongba ophiolite, Yarlung Zangbo Suture Zone: Implications for the Early Cretaceous intra-oceanic subduction zone within the Neo-Tethys: *Chemical Geology*, v. 288, p. 133–148. [10.1016/j.chemgeo.2011.07.011](https://doi.org/10.1016/j.chemgeo.2011.07.011)
- Dai, J.G., Wang, C.S., Hourigan, J.K., and Santosh, M., 2013, Insights into the early Tibetan Plateau from (U–Th)/He thermochronology: *Journal of the Geological Society*, v. 170, no. 6, p. 917–927. [10.1144/jgs2012-076](https://doi.org/10.1144/jgs2012-076)
- Dickin, A.P., 2005, *Radiogenic Isotope Geology[M]//Radiogenic isotope geology*: Cambridge, Cambridge University Press, p. 60.
- Ewart, A., Milner, S.C., and Armstrong, R.A., 1998, Erendeka volcanism of the Goboboseb mountains and Messum igneous complex, Namibia, part I: Geochemical evidence of early Cretaceous Tristan Plume melts and the role of crustal contamination in the Parana–Etendeka CFB: *Journal of Petrology*, v. 39, p. 191–225. [10.1093/ptro/39.2.191](https://doi.org/10.1093/ptro/39.2.191)
- Falloon, T.J., Berry, R.F., Robinson, P., and Stolz, A.J., 2006, Whole-rock geochemistry of the Hili Manu peridotite, east

- Timor: Implications for the origin of Timor ophiolites: *Australian Journal of Earth Sciences*, v. 53, no. 4, p. 637–649. [10.1080/08120090600686793](https://doi.org/10.1080/08120090600686793)
- Fan, J.J., Li, C., Liu, Y.M., and Xu, J.X., 2015, Age and nature of the late Early Cretaceous Zhaga Formation, northern Tibet: Constraints on when the Bangong-Nujiang Neo-Tethys Ocean closed: *International Geology Review*, v. 57, no. 3, p. 342–353. [10.1080/00206814.2015.1006695](https://doi.org/10.1080/00206814.2015.1006695)
- Frey, F.A., Green, D.H., and Roy, S.D., 1978, Integrated models of basalt petrogenesis: A study of quartz tholeiites to olivine melilitites from southeastern Australia utilizing geochemical and experimental petrological data: *Journal of Petrology*, v. 19, p. 463–513. [10.1093/petrology/19.3.463](https://doi.org/10.1093/petrology/19.3.463)
- Gibson, I.L., Kirkpatrick, R.J., Emmerman, R., Schmincke, H.U., Pritchard, G., Oakley, P.J., Thorpe, R.S., and Marriner, G.F., 1982, The trace element composition of the lavas and dikes from a 3-km vertical section through the lava pile of Eastern Iceland: *Journal of Geophysical Research*, v. 87, no. B8, p. 6532–6546. doi:[10.1029/JB087iB08p06532](https://doi.org/10.1029/JB087iB08p06532)
- Griffin, W.L., Pearson, N.J., Belousova, E., Jackson, S.E., O'Reilly, S.Y., Achterberg, E., and Shee, S.R., 2000, The Hf-isotope composition of cratonic mantle: LAM-MC-ICPMS analysis of zircon megacrysts in kimberlites: *Geochimica Et Cosmochimica Acta*, v. 64, p. 133–147. [10.1016/S0016-7037\(99\)00343-9](https://doi.org/10.1016/S0016-7037(99)00343-9)
- Griffin, W.L., Wang, X., Jackson, S.E., Pearson, N.J., O'Reilly, S.Y., Xu, X.S., and Zhou, X.M., 2002, Zircon chemistry and magma mixing, SE china: In-situ analysis of Hf isotopes, Tonglu and Pingtan igneous complexes: *Lithos*, v. 61, no. 3, p. 237–269. doi:[10.1016/S0024-4937\(02\)00082-8](https://doi.org/10.1016/S0024-4937(02)00082-8)
- Guyon, J.H., Kapp, P., Pullen, A., Herzler, M., Gehrels, G., and Lin, D., 2006, Tibetan basement rocks near Amdo reveal “missing” Mesozoic tectonism along the Bangong suture, central Tibet: *Geology*, v. 34, no. 6, p. 505–508. doi:[10.1130/G22453.1](https://doi.org/10.1130/G22453.1)
- Hao, L.L., Wang, Q., Wyman, D.A., Quan, O., Dan, W., Jiang, Z. Q., Wu, F.Y., Yang, J.S., Long, X.P., and Li, J., 2015, Underplating of basaltic magmas and crustal growth in a continental arc: Evidence from Late Mesozoic intermediate-felsic intrusive rocks in southern Qiangtang, central Tibet: *Lithos*, v. 245, p. 223–242. [10.1016/j.lithos.2015.09.015](https://doi.org/10.1016/j.lithos.2015.09.015)
- Hasenclever, J., Phipps, M.J., and Hort, M., 2005, Implications of a plume-fed asthenosphere layer for mantle flow and mid-ocean ridge melting processes: AGU Fall Meeting Abstracts, 2005.
- Hawkins, J.W., 2003, Geology of supra-subduction zones—implications for the origin of ophiolites, in Dilek, Y., and Newcomb, S., eds., *Ophiolite concept and the evolution of geological thought*, volume Vol. 373: Boulder, CO, Geological Society of America Special Paper, p. 227–268.
- Hu, F.F., Fan, H.R., Yang, J.H., Zhai, M.G., Jin, C.W., Xie, L.W., and Yang, Y.H., 2005, Magma mixing for the origin of granodiorite: Geochemical, Sr-Nd isotopic and zircon Hf isotopic evidence of dioritic enclaves and host rocks from Changshannan granodiorite in the Jiaodong Peninsula, eastern China: *Acta Petrologica Sinica*, v. 21, no. 3, p. 569–586. [In Chinese with English abstract.]
- Hu, X.C., Xia, B., Huang, Q.T., Liu, W.L., Zhong, Y., Yuan, Y.J., Xia, L.Z., Wu, Y., and Zhang, X., 2016, Geochemistry, geochronology, and petrogenesis of mid-Cretaceous Talabuco volcanic rocks, central Tibet: Implications for the evolution of the Bangong Meso-Tethys: *International Geology Review*, p. 484–501. [10.1080/00206814.2016.1230524](https://doi.org/10.1080/00206814.2016.1230524)
- Huang, Q.S., Shi, R.D., Liu, D.L., Zhang, X.R., Fan, S.Q., and Ding, L., 2013, Os isotopic evidence for a carbonaceous chondritic mantle source for the Nagqu ophiolite from Tibet and its implications: *Science Bulletin*, v. 58, no. 1, p. 92–98. [In Chinese with English abstract.]. [10.1007/s11434-012-5384-8](https://doi.org/10.1007/s11434-012-5384-8)
- Huang, Q.S., Shi, R.D., O'Reilly, S.Y., Griffin, W.L., Zhang, M., Liu, D.L., and Zhang, X.R., 2015a, Re-Os isotopic constraints on the evolution of the Bangong-Nujiang Tethyan oceanic mantle: *Central Tibet: Lithos*, v. 32-45, p. 224–225.
- Huang, Q.T., Li, J.F., Cai, Z.R., Xia, L.Z., Yuan, Y.J., Liu, H.C., and Xia, B., 2015b, Geochemistry, Geochronology, Sr-Nd Isotopic Compositions of Jiang Tso Ophiolite in the Middle Segment of the Bangong-Nujiang Suture Zone and Their Geological Significance: *Acta Geologica Sinica*, v. 89, no. 2, p. 389–401. [In Chinese with English abstract.]. [10.1111/1755-6724.12437](https://doi.org/10.1111/1755-6724.12437)
- Huang, Y., Zhu, D.C., Zhao, Z.D., Zhang, L.L., DePaolo, D., Hu, Z. C., Yuan, H.L., and Mo, X.X., 2012, Petrogenesis and implication of the andesites at ~113 Ma in the Nagqu region in the northern Lhasa subterrane: *Acta Petrologica Sinica*, v. 28, p. 1603–1614. [In Chinese with English abstract.]
- Ji, W.Q., Wu, F.Y., Chung, S.L., Li, J.X., and Liu, C.Z., 2009, Zircon U-Pb chronology and Hf isotopic constraints on the petrogenesis of Gangdese batholiths, southern Tibet: *Chemical Geology*, v. 262, p. 229–245. [10.1016/j.chemgeo.2009.01.020](https://doi.org/10.1016/j.chemgeo.2009.01.020)
- Kang, Z.Q., Xu, J.F., Dong, Y.H., and Wang, B.D., 2008, Cretaceous volcanic rocks of Zenong Group in north-middle Lhasa block: Products of southward subducting of the Slainajap ocean?: *Acta Petrologica Sinica*, v. 24, no. 2, p. 303–314. [In Chinese with English abstract.]
- Kang, Z.Q., Xu, J.F., Wilde, S.A., Feng, Z.H., Chen, J.L., Wang, B. D., Fu, W.C., and Pan, H.B., 2014, Geochronology and geochemistry of the Sangri Group Volcanic Rocks, Southern Lhasa Terrane: Implications for the early subduction history of the Neo-Tethys and Gangdese Magmatic Arc: *Lithos*, v. 200, p. 157–168. [10.1016/j.lithos.2014.04.019](https://doi.org/10.1016/j.lithos.2014.04.019)
- Kapp, P., Yin, A., Harrison, T.M., and Lin, D., 2005, Cretaceous-Tertiary shortening, basin development, and volcanism in central Tibet: *Geological Society of America Bulletin*, v. 117, p. 865–878. [10.1130/B25595.1](https://doi.org/10.1130/B25595.1)
- Kepezhinskas, P., McDermott, F., Defant, M.J., Hochstaedter, A., Drummond, M.S., Hawkesworth, C.J., Koloskov, A., Maury, R. C., and Bellon, H., 1997, Trace element and Sr-Nd-Pb isotopic constraints on a three-component model of Kamchatka arc petrogenesis: *Geochimica Et Cosmochimica Acta*, v. 61, p. 577–600. [10.1016/S0016-7037\(96\)00349-3](https://doi.org/10.1016/S0016-7037(96)00349-3)
- Kong, F.M., Su, W., Li, X.P., and Li, S.J., 2012, Geochemistry of the Dongdegou Peridotites in Southwestern Tianshan Mountains and Its Geological Significance: *Geological Review*, v. 58, no. 6, p. 1161–1174. [In Chinese with English abstract.]
- LaFlèche, M.R., Camiré, G., and Jenner, G.A., 1998, Geochemistry of post-Acadian, Carboniferous continental intraplate basalts from the Maritimes basin, Magdalen islands, Québec, Canada: *Chemical Geology*, v. 148, p. 115–136. [10.1016/S0009-2541\(98\)00002-3](https://doi.org/10.1016/S0009-2541(98)00002-3)
- Lai, S.C., and Liu, C.Y., 2003, Geochemistry and genesis of the island-arc ophiolite in Anduo area, Tibetan plateau: *Acta*

- Petrologica Sinica, v. 19, no. 4, p. 675–682. [In Chinese with English abstract.]
- Leshner, C.E., 1990, Decoupling of chemical and isotopic exchange during magma mixing: *Nature*, v. 344, no. 6263, p. 235–237. [10.1038/344235a0](https://doi.org/10.1038/344235a0)
- Li, C.Y., Zhang, H., Wang, F.Y., Liu, J.Q., Sun, Y.L., Hao, X.L., Li, Y. L., and Sun, W., 2012, The formation of the Dabaoshan porphyry molybdenum deposit induced by slab rollback: *Lithos*, v. 150, p. 101–110. [10.1016/j.lithos.2012.04.001](https://doi.org/10.1016/j.lithos.2012.04.001)
- Li, X.H., Long, W.G., Li, Q.L., Liu, Y., Zheng, Y.F., Yang, Y.H., Clamberlain, K.R., Wan, D.F., Guo, C.H., Wang, X.C., and Tao, H., 2010, Penglai zircon megacrysts: A potential new working reference material for microbeam determination of Hf-O isotopes and U-Pb age: *Geostandards and Geoanalytical Research*, v. 34, no. 2, p. 117–134. doi:[10.1111/j.1751-908X.2010.00036.x](https://doi.org/10.1111/j.1751-908X.2010.00036.x)
- Li, Y.L., He, J., Wang, C.S., Han, Z.P., Ma, P.F., Xu, M., and Du, K. Y., 2014, Cretaceous volcanic rocks in south Qiangtang Terrane: Products of northward subduction of the Bangong-Nujiang Ocean?: *Journal of Asian Earth Sciences*, v. 104, p. 69–83. [10.1016/j.jseae.2014.09.033](https://doi.org/10.1016/j.jseae.2014.09.033)
- Lightfoot, P.C., Hawkesworth, C.J., Hergt, J., Naldrett, A.J., Gorbachev, N.S., Fedorenko, V.A., and Doherty, W., 1993, Remobilisation of the continental lithosphere by a mantle plume: Major-trace-element, and Sr, Nd and Pb-isotope evidence from picritic and tholeiitic lavas of the Noril'sk District, Siberian Trap, Russia: *Contributions to Mineralogy and Petrology*, v. 114, p. 171–188. [10.1007/BF00307754](https://doi.org/10.1007/BF00307754)
- Liu, D.L., Huang, Q.S., Fan, S.Q., Zhang, L.Y., Shi, R.D., and Ding, L., 2014, Subduction of the Bangong-Nujiang Ocean: Constraints from granites in the Bangong Co area, Tibet: *Geological Journal*, v. 49, p. 188–206. [10.1002/gj.2510](https://doi.org/10.1002/gj.2510)
- Liu, T., Zhai, Q.G., Wang, J., Bao, P.S., Qiangba, Z.X., Tang, S.H., and Tang, Y., 2016, Tectonic significance of the Dongqiao ophiolite in the north-central Tibetan plateau: Evidence from zircon dating, petrological, geochemical and Sr-Nd-Hf isotopic characterization: *Journal of Asian Earth Sciences*, v. 116, p. 139–154. [10.1016/j.jseae.2015.11.014](https://doi.org/10.1016/j.jseae.2015.11.014)
- Liu, Y., Gao, S., Hu, Z., Gao, C., Zong, K., and Wang, D., 2010, Continental and oceanic crust recycling-induced melt-peridotite interactions in the Trans-North China Orogen: U-Pb dating, Hf isotopes and trace elements in zircons from mantle xenoliths: *Journal of Petrology*, v. 51, no. 1–2, p. 537–571. doi:[10.1093/petrology/egp082](https://doi.org/10.1093/petrology/egp082)
- Liu, Y.M., Li, C., Xie, C.M., Wang, M., and Fan, J.J., 2017a, Geochronology of the Duguer range metamorphic rocks, Central Tibet: Implications for the changing tectonic setting of the South Qiangtang subterranean: *International Geology Review*, v. 59, p. 29–44. [10.1080/00206814.2016.1199977](https://doi.org/10.1080/00206814.2016.1199977)
- Liu, Y.M., Wang, M., Li, C., and Sun, Z.M., 2017b, Cretaceous structures in the Duolong region of central Tibet: Evidence for an accretionary wedge and closure of the Bangong-Nujiang Neo-Tethys Ocean: *Gondwana Research*, v. 48. [10.1016/j.gr.2017.04.026](https://doi.org/10.1016/j.gr.2017.04.026)
- Liu, Y.S., Hu, Z.C., Gao, S., Günther, D., Xu, J., Gao, C.G., and Chen, H.H., 2008, In situ analysis of major and trace elements of anhydrous minerals by LA-ICP-MS without applying an internal standard: *Chemical Geology*, v. 257, no. 1–2, p. 34–43. doi:[10.1016/j.chemgeo.2008.08.004](https://doi.org/10.1016/j.chemgeo.2008.08.004)
- Ludwing, K.R., 2003, *Isoplot, A Geochronological Toolkit for Microsoft Excel*: Berkeley, Special Publication, Berkeley Geochronology Center, p. 1–70.
- McKenzie, D., and Bickle, M.J., 1988, The volume and composition of melt generated by extension of the lithosphere: *Journal of Petrology*, v. 29, no. 3, p. 625–679. doi:[10.1093/petrology/29.3.625](https://doi.org/10.1093/petrology/29.3.625)
- Meng, F.X., Gao, S., Niu, Y.L., Liu, Y.S., and Wang, X.R., 2015, Mesozoic-Cenozoic mantle evolution beneath the North China Craton: A new perspective from Hf-Nd isotopes of basalts: *Gondwana Research*, v. 27, p. 1574–1585. [10.1016/j.gr.2014.01.014](https://doi.org/10.1016/j.gr.2014.01.014)
- Miller, C., Thoni, M., Frank, W., Schuster, R., Melcher, F., Meisel, T., and Zanetti, A., 2003, Geochemistry and tectonomagmatic affinity of the Yungbwa ophiolite, SW Tibet: *Lithos*, v. 66, p. 155–172. [10.1016/S0024-4937\(02\)00217-7](https://doi.org/10.1016/S0024-4937(02)00217-7)
- Miyashiro, A., 1974, Volcanic rock series in island arcs and active continental margins: *American Journal of Science*, v. 274, no. 4, p.321–355. [10.2475/ajs.274.4.321](https://doi.org/10.2475/ajs.274.4.321)
- Mo, X.X., Dong, G.C., Zhao, Z.D., Zhou, S., Wang, L.L., Qiu, R.Z., and Zhang, F.Q., 2005, Spatial and temporal distribution and characteristics of granitoids in the Gangdese, Tibet and implication for crustal growth and evolution: *Geological Journal of China Universities*, v. 11, p. 281–290. [In Chinese with English abstract.]
- Niu, Y.L., 2004, Bulk-rock major and trace element compositions of abyssal peridotites: Implications for mantle melting, melt extraction and post-melting processes beneath mid-ocean ridges: *Journal of Petrology*, v. 45, p. 2423–2458. [10.1093/petrology/egh068](https://doi.org/10.1093/petrology/egh068)
- Pan, G.T., Chen, Z.L., Li, X.Z., Yan, Y.J., Xu, X.S., Xu, Q., Jiang, X.S., Wu, Y.L., Luo, J.L., Zhu, T.X., and Peng, Y.M., 1997, Geological-tectonic evolution in the eastern Tethys: Beijing, Geological Publishing House. [In Chinese with English abstract.]
- Pan, G.T., Mo, X.X., Hou, Z.Q., Zhu, D.C., Wang, L.Q., Li, G.M., Zhao, Z.D., Geng, Q.R., and Liao, Z.L., 2006, Spatial-temporal framework of the Gangdese Orogenic Belt and its evolution: *Acta Petrologica Sinica*, v. 22, p. 521–533. [In Chinese with English abstract.]
- Pan, G.T., Wang, L.Q., Li, R.S., Yuan, S.H., Ji, W.H., Yin, F.G., Zhang, W.P., and Wang, B.D., 2012, Tectonic evolution of the Qinghai-Tibet Plateau: *Journal of Asian Earth Sciences*, v. 53, p. 3–14. [10.1016/j.jseae.2011.12.018](https://doi.org/10.1016/j.jseae.2011.12.018)
- Parkinson, I., and Pearce, J., 1998, Peridotites from the Izu-Bonin-Mariana forearc (ODP Leg125): Evidence for mantle melting and melt-mantle interaction in a supra-subduction zone setting: *Journal of Petrology*, v. 39, p. 1577–1618. [10.1093/petroj/39.9.1577](https://doi.org/10.1093/petroj/39.9.1577)
- Paulick, H., Bach, W., Godard, M., De Hoog, J.C.M., Suhr, G., and Harvey, J., 2006, Geochemistry of abyssal peridotites (Mid-Atlantic Ridge, 15° 20' N, ODP Leg 209): Implications for fluid/rock interaction in slow spreading environments: *Chemical Geology*, v. 234, p. 179–210. [10.1016/j.chemgeo.2006.04.011](https://doi.org/10.1016/j.chemgeo.2006.04.011)
- Pearce, J.A., Barker, P.F., Edwards, S.J., Parkinson, I.J., and Leat, P.T., 2000, Geochemistry and tectonic significance of peridotites from the South Sandwich arc-basin system, South Atlantic: *Contributions to Mineralogy and Petrology*, v. 139, p. 36–53. [10.1007/s004100050572](https://doi.org/10.1007/s004100050572)
- Pearce, J.A., and Cann, J.R., 1973, Tectonic setting of basic volcanic rocks determined using trace element analyses: *Earth and Planetary Science Letters*, v. 19, p. 290–300. [10.1016/0012-821X\(73\)90129-5](https://doi.org/10.1016/0012-821X(73)90129-5)
- Pearce, J.A., and Deng, W.M., 1988, The ophiolites of the Tibet geotraverse, Lhasa to Golmud (1985) and Lhasa to

- Kathmandu (1986): Philosophical Transactions of the Royal Society, A: Mathematical, Physical and Engineering Sciences, v. 327, p. 215–238. [10.1098/rsta.1988.0127](https://doi.org/10.1098/rsta.1988.0127)
- Pearce, J.A., 1983, Role of subduction lithosphere in magma genesis at active continental margins, in Hawkesworth, C.J., and Nory, M.J., Eds., *Continental Basalts and Mantle Xenoliths*: Cheshire, UK, Shiva, p. 230–249.
- Pearce, J.A., Lippard, S.J., and Roberts, S., 1984, Characteristics and tectonic significance of supra subduction zone ophiolites: London, Geological Society, Special Publications, v. 16, no. 1, p. 77–94.
- Pearce, J.A., and Norry, M.J., 1979, Petrogenetic implications of Ti, Zr, Y, and Nb variations in volcanic rocks: *Contributions to Mineralogy and Petrology*, v. 69, no. 1, p. 33–47. doi:[10.1007/BF00375192](https://doi.org/10.1007/BF00375192)
- Pearce, J.A., and Peate, D.W., 1995, Tectonic implications of the composition of volcanic arc magmas: *Annual Review of Earth and Planetary Sciences*, v. 23, p. 251–285. [10.1146/annurev.ea.23.050195.001343](https://doi.org/10.1146/annurev.ea.23.050195.001343)
- Plank, T., 2005, Constraints from thorium/lanthanum on sediment recycling at subduction zones and the evolution of the continents: *Journal of Petrology*, v. 46, p. 921–944. [10.1093/petrology/egj005](https://doi.org/10.1093/petrology/egj005)
- Plank, T., 2014, 4.17-The Chemical Composition of Subducting Sediments: *Treatise on Geochemistry*, p.607–629
- Qi, L., and Grégoire, D.C., 2000, Determination of trace elements in twenty six Chinese geochemistry reference materials by inductively coupled plasma-mass spectrometry: *Geostandards and Geoanalytical Research*, v. 24, p. 51–63. [10.1111/j.1751-908X.2000.tb00586.x](https://doi.org/10.1111/j.1751-908X.2000.tb00586.x)
- Reagan, M.K., Ishizuka, O., Kelley, K.A., Ohara, Y., Blichert-Toft, J., Bloomer, S.H., Cash, J., Fryer, P., Hanan, B.B., Hickey-Vargas, R., Ishii, T., Kimura, J.I., Peate, D.W., Rowe, M.C., and Woods, M., 2010, Fore-arc basalts and subduction initiation in the Izu-Bonin-Mariana system: *Geochemistry, Geophysics, Geosystems*, v. 11, no. 3, p. 1–17, Q03X12. doi:[10.1029/2009GC002871](https://doi.org/10.1029/2009GC002871).
- Saunders, A.D., Storey, M., Kent, R.W., and Norry, M.J., 1992, Consequences of plume-lithosphere interactions, in Storey, B.C., Alabaster, T., and Pankhurst, R.J., Eds., *Magmatism and the Cause of Continental Breakup*, volume Vol. 68: London, Geological Society of Special Publication, p. 41–60.
- Scherer, E., Münker, C., and Mezger, K., 2001, Calibration of the Lutetium-Hafnium Clock: *Science*, v. 293, no. 5530, p. 683. doi:[10.1126/science.1061372](https://doi.org/10.1126/science.1061372)
- Scherer, E.E., Cameron, K.L., and Blichert-Toft, J., 2000, Lu-Hf garnet geochronology: Closure temperature relative to the Sm-Nd system and the effects of trace mineral inclusions: *Geochimica Et Cosmochimica Acta*, v. 64, no. 19, p. 3413–3432. [10.1016/S0016-7037\(00\)00440-3](https://doi.org/10.1016/S0016-7037(00)00440-3)
- Shervais, J.W., 1982, Ti-V plots and the petrogenesis of modern and ophiolitic lavas: *Earth and Planetary Science Letters*, v. 59, p. 101–118. [10.1016/0012-821X\(82\)90120-0](https://doi.org/10.1016/0012-821X(82)90120-0)
- Shi, R.D., Griffin, W.L., O'Reilly, S.Y., Huang, Q.S., Zhang, X.R., Liu, D.L., Zhi, X.C., Xia, Q.X., and Ding, L., 2012, Melt/mantle mixing produces podiform chromite deposits in ophiolites: Implications of Re-Os systematics in the Dongqiao Neotethyan ophiolite, northern Tibet: *Gondwana Research*, v. 21, p. 194–206. [10.1016/j.gr.2011.05.011](https://doi.org/10.1016/j.gr.2011.05.011)
- Shi, R.D., Griffin, W.L., O'Reilly, S.Y., Zhang, X.R., Huang, Q.S., Gong, X.H., and Ding, L., 2013, Geodynamic constraints on the recycling of ancient SCLM and genesis of Tibetan diamondiferous ophiolites: Goldschmidt 2013 Conference Abstracts, p. 2196.
- Shinjo, R., Chung, S.-L., Kato, Y., and Kimura, M., 1999, Geochemical and Sr-Nd isotopic characteristics of volcanic rocks from the Okinawa Trough and Ryukyu Arc: Implications for the evolution of a young, intracontinental back arc basin: *Journal of Geophysical Research: Solid Earth*, v. 104, no. B5, p. 10591–10608. doi:[10.1029/1999JB900040](https://doi.org/10.1029/1999JB900040)
- Sui, Q.L., Wang, Q., Zhu, D.C., Zhao, Z.D., Chen, Y., Santosh, M., Hu, C.Z., Yuan, H.L., and Mo, X.X., 2013, Compositional diversity of ca. 110 Ma magmatism in the northern Lhasa Terrane, Tibet: Implications for the magmatic origin and crustal growth in a continent-continent collision zone: *Lithos*, v. 168–169, p. 144–159. [10.1016/j.lithos.2013.01.012](https://doi.org/10.1016/j.lithos.2013.01.012)
- Sun, L.X., Bai, Z.D., Xun, D.B., Li, H.K., and Sun, B., 2011, Geological Characteristics and Zircon U-Pb SHRIMP Dating of the Plagiogranite in Amduo ophiolites, Tibet: *Geological Survey and Research*, v. 34, no. 1, p. 10–15. [In Chinese with English abstract.]
- Sun, S.S., and McDonough, W.F., 1989, Chemical and isotopic systematics of oceanic basalt: Implication for mantle composition and processes, in Saunders, A.D., and Morry, M.J., Eds., *Magmatism in the Ocean Basin*, volume Vol. 42: Geological Society of London Special Publication, p. 528–548. [10.1144/GSL.SP.1989.042.01.19](https://doi.org/10.1144/GSL.SP.1989.042.01.19)
- Tang, Y., Zhai, Q.G., Liu, T., Wang, J., Hu, P.Y., Qiangba, Z.X., and Suolang, C.L., 2015, LA-ICP-MS zircon U-Pb dating, geochemical features and geological significance of the Daru Co granite porphyry in Baingoin County, Tibet: *Geological Bulletin of China*, v. 34, no. 10, p. 1802–1811. [In Chinese with English abstract.]
- Taylor, S.R., and McLennan, S.M., 1995, The geochemical evolution of the continental crust: *Reviews of Geophysics*, v. 33, no. 2, p. 241–265. doi:[10.1029/95RG00262](https://doi.org/10.1029/95RG00262)
- Thirlwall, M.F., 1991, Long-term reproducibility of multicollector Sr and Nd isotope ratio analysis: *Chemical Geology Isotope Geoscience*, v. 94, no. 2, p. 85–104. [10.1016/0168-9622\(91\)90002-E](https://doi.org/10.1016/0168-9622(91)90002-E)
- Tian, L.Y., Castillo, P.R., Hawkins, J.W., Hilton, D.R., Hanan, B.B., and Pietruszka, A.J., 2008, Major and trace element and Sr-Nd isotope signatures of lavas from the Central Lau Basin: Implications for the nature and influence of subduction components in the back-arc mantle: *Journal of Volcanology and Geothermal Research*, v. 178, p. 657–670. [10.1016/j.jvolgeores.2008.06.039](https://doi.org/10.1016/j.jvolgeores.2008.06.039)
- Tilton, G.R., 1960, Volume diffusion as a mechanism for discordant lead ages: *Journal of Geophysical Research*, v. 65, no. 9, p. 2933–2945. doi:[10.1029/JZ065i009p02933](https://doi.org/10.1029/JZ065i009p02933)
- Wang, B.D., Wang, L.Q., Chung, S.L., Chen, J.L., Yin, F.G., Liu, H., Li, X.B., and Chen, L.K., 2016, Evolution of the Bangong-Nujiang Tethyan ocean: Insights from the geochronology and geochemistry of mafic rocks within ophiolites: *Lithos*, v. 245, p. 18–33. [10.1016/j.lithos.2015.07.016](https://doi.org/10.1016/j.lithos.2015.07.016)
- Wang, X.B., Bao, P.S., Deng, W.M., and Wang, W.G., 1987, Xizang (Tibet) ophiolites: Beijing, Geological Publishing House. [In Chinese with English abstract.]
- Wang, X.C., Xia, B., Liu, W.L., Zhong, Y., Hu, X.C., Guan, Y., Huang, W., and Yin, Z.X., 2017, Geochronology, geochemistry and petrogenesis of the Pungco ophiolite: Tibet, *Geotectonic Et Metallogenia*. [In Chinese with English abstract, in press.]

- Wang, Z.H., Wang, Y.S., Xie, Y.H., Sun, Z.G., Lu, Z.L., Qu, Y.G., Li, C.Z., and Jiang, X.F., 2005, The Tarenben oceanic-island basalts in the middle part of the Bangong-Nujiang suture zone, Xizang and their geological implications: *Sedimentary Geology and Tethyan Geology*, v. 25, no. 1–2, p. 155–162. [In Chinese with English abstract.]
- Wedepohl, K.H., 1995, The composition of the continental crust: *Geochimica Et Cosmochimica Acta*, v. 59, p. 1217–1232. [10.1016/0016-7037\(95\)00038-2](https://doi.org/10.1016/0016-7037(95)00038-2)
- Wei, Z.Q., Xia, B., Xu, L.F., Wang, R., and Zhou, G.Q., 2009, Geochemistry and tectonic setting of Western Pungco Lake Ophiolite, Xizang (Tibet): *Geological Review*, v. 55, p. 785–793.
- Wetherill, G.W., 1956, Discordant uranium-lead ages, I: *Eos, Transactions American Geophysical Union*, v. 37, no. 3, p. 320–326. [10.1029/TR037i003p00320](https://doi.org/10.1029/TR037i003p00320)
- Winchester, J.A., and Floyd, P.A., 1977, Geochemical discrimination of different magma series and their differentiation products using immobile elements: *Chemical Geology*, v. 20, p. 325–343. [10.1016/0009-2541\(77\)90057-2](https://doi.org/10.1016/0009-2541(77)90057-2)
- Wood, D.A., Joron, J.L., and Treuil, M., 1979, A re-appraisal of the use of trace elements to classify and discriminate between magma series erupted in different tectonic settings: *Earth and Planetary Science Letters*, v. 45, no. 2, p. 326–336. doi:[10.1016/0012-821X\(79\)90133-X](https://doi.org/10.1016/0012-821X(79)90133-X)
- Wu, F.Y., Li, X.H., Zheng, Y.F., and Gao, S., 2006, Lu-Hf isotopic systematics and their applications in petrology: *Acta Petrologica Sinica*, v. 23, no. 2, p. 185–220. [In Chinese with English abstract.]
- Xia, B., Li, J.F., Liu, L.W., Xu, L.F., He, G.S., Wang, H., Zhang, Y.Q., and Yang, Z.Q., 2008, SHRIMP U-Pb dating for dolerite in Sangsang ophiolite, Xizang, China: Geochronological constraint for development of eastern Tethys basin: *Geochimica*, v. 37, p. 399–403. [In Chinese with English abstract.]
- Xiao, L., Xu, Y.G., Mei, H.J., Zheng, Y.F., He, B., and Pirajno, F., 2004, Distinct mantle sources of low-Ti and high-Ti basalts from the western Emeishan large igneous province, SW China: Implications for plume-lithosphere interaction: *Earth and Planetary Science Letters*, v. 228, no. 3–4, p. 525–546. [10.1016/j.epsl.2004.10.002](https://doi.org/10.1016/j.epsl.2004.10.002)
- Xiao, X.C., and Li, Y.D., 2000, Tectonic and evolution and uplift of Qinghai-Xizang (Tibet) Plateau: Guangzhou, Guangdong Science and Technology Press, p. 1–313. [In Chinese with English abstract.]
- Xizang Geological Survey Institute, 2003a, The regional geological survey of 1: 250000 Bangor Sheet, Unpublished. [In Chinese.]
- Xizang Geological Survey Institute, 2003b, The regional geological survey of 1: 250000 Zigetangco Sheet, Unpublished. [In Chinese.]
- Xizang Geological Survey Institute, 2005, The regional geological survey of 1: 250000 Nagqu Sheet, Unpublished. [In Chinese.]
- Xu, L.F., Xia, B., Li, J.F., and Zhong, L.F., 2010, Geochemical characteristics and genesis of pillow basalts from the Lanong ophiolite in Tibet, China: *Geotectonica Et Metallogenia*, v. 34, no. 1, p. 105–113. [In Chinese with English abstract.]
- Xu, R.H., Schärer, U., and Allègre, C.J., 1985, Magmatism and metamorphism in the Lhasa block (Tibet): A chronological study: *Journal of Geology*, v. 93, p. 41–57. [10.1086/628918](https://doi.org/10.1086/628918)
- Xu, R.K., Zheng, Y.Y., Zhao, P.J., Shan, L., Zhang, Y.L., Cao, L., Qi, J.H., Zhang, G.Y., and Dai, F.H., 2007, Definition and geological significance of the Gacangjian volcanic arc north of Dongqiao, Tibet: *Geology in China*, v. 1, no. 3, p. 199–205. [In Chinese with English abstract.]
- Yang, R.H., Cai, L., Chi, X.G., and Wang, T.W., 2003, The primary study of geochemical characteristics and tectonic setting of ophiolite in Yongzhu-Namuhu, Tibet: *Geoscience*, v. 17, no. 1, p. 14–19. [In Chinese with English abstract.]
- Ye, P.S., 2004, Ophiolites and thrust system of middle Lhasa block: Beijing, Chinese Academy of Geological Sciences, p. 1–126. [In Chinese with English abstract.]
- Ye, P.S., Wu, Z.H., Hu, D.G., Jiang, W., Liu, Q.S., and Yang, X.D., 2004, Geochemical characteristics and tectonic setting of ophiolite of Dongqiao, Tibet: *Geoscience*, v. 18, no. 3, p. 309–315. [In Chinese with English abstract.]
- Yi, M.X., Zhao, Y.Y., Wang, A., Xu, H., Li, X.S., Lu, W., and Wang, X.W., 2017, LA-MC-ICP-MS U-Pb Dating of Orthopyre from the Jiangcuo Iron Deposit in Baingoin County, Tibet and its Geological Significance: *Acta Geological Sinica*, v. 91, no. 5, p. 1039–1051. [In Chinese with English abstract.]
- Yin, A., and Harrison, T.M., 2000, Geologic evolution of the Himalayan-Tibetan orogen: *Annual Review of Earth and Planetary Sciences*, v. 28, p. 211–280. [10.1146/annurev.earth.28.1.211](https://doi.org/10.1146/annurev.earth.28.1.211)
- Zeng, M., Zhang, X., Cao, H., Etensohn, F.R., Chen, W.B., and Lang, X.H., 2015, Late Triassic initial subduction of the Bangong-Nujiang Ocean beneath Qiangtang revealed: Stratigraphic and geochronological evidence from Gaize Tibet: *Basin Research*, v. 28, no. 1, p. 1–11. doi:[10.1111/bre.12105](https://doi.org/10.1111/bre.12105)
- Zeng, Y.C., Chen, J.L., Xu, J.F., and Huang, F., 2016, Sediment melting during subduction initiation: Geochronological and geochemical evidence from the Darutso high-Mg andesites within ophiolite melange, central Tibet: *Geochimica Geophysica Geosystems*, v. 17, no. 12, p. 4859–4877. doi:[10.1002/2016GC006456](https://doi.org/10.1002/2016GC006456)
- Zhang, K.J., Xia, B., Zhang, Y.X., Liu, W.L., Zeng, L., Li, J.F., and Xu, L.F., 2014a, Central Tibetan Meso-Tethyan oceanic plateau: *Lithos*, v. 210–211, p. 278–288. [10.1016/j.lithos.2014.09.004](https://doi.org/10.1016/j.lithos.2014.09.004)
- Zhang, K.J., Xia, B.D., Wang, G.M., Li, Y.T., and Ye, H.F., 2004, Early Cretaceous stratigraphy. Depositional Environment, sandstone provenance, and tectonic setting of central Tibet, western China: *Geological Society of America Bulletin*, v. 116, p. 1202–1222. [10.1130/B25388.1](https://doi.org/10.1130/B25388.1)
- Zhang, X.R., Shi, R.D., Huang, Q.S., Liu, D.L., Gong, X.H., Chen, S.S., Wu, K., Yi, G.D., Sun, Y.L., and Ding, L., 2014c, Early Jurassic high-pressure metamorphism of the Amdo terrane, Tibet: Constraints from zircon U-Pb geochronology of mafic granulites: *Gondwana Research*, v. 26, p. 975–985. [10.1016/j.gr.2013.08.003](https://doi.org/10.1016/j.gr.2013.08.003)
- Zhang, Y.X., Li, Z.W., Yang, W.G., Zhu, L.D., Jin, X., Zhou, X.Y., Tao, G., and Zhang, K.J., 2017, Late Jurassic-Early Cretaceous episodic development of the Bangong Meso-Tethyan subduction: Evidence from elemental and Sr-Nd isotopic geochemistry of arc magmatic rocks, Gaize region, central Tibet, China: *Journal of Asian Earth Sciences*, v. 135, p. 212–242. [10.1016/j.jseaes.2016.12.043](https://doi.org/10.1016/j.jseaes.2016.12.043)
- Zhang, Y.X., and Zhang, K.J., 2017, Early Permian Qiangtang flood basalts, northern Tibet, China: A mantle plume that disintegrated northern Gondwana?: *Gondwana Research*, v. 44, p. 96–108. [10.1016/j.gr.2016.10.019](https://doi.org/10.1016/j.gr.2016.10.019)
- Zhang, Z.M., Dong, X., Liu, F., Lin, Y.H., Yan, R., and Santosh, M., 2012, Tectonic evolution of the Amdo terrane, central Tibet:

- Petrochemistry and zircon U-Pb geochronology: *Journal of Geology*, v. 120, p. 431–451. [10.1086/665799](https://doi.org/10.1086/665799)
- Zhang, Z.M., Dong, X., Santosh, M., and Zhao, G.C., 2014b, Metamorphism and tectonic evolution of the Lhasa terrane, Central Tibet: *Gondwana Research*, v. 25, p. 170–189. [10.1016/j.gr.2012.08.024](https://doi.org/10.1016/j.gr.2012.08.024)
- Zhao, J.H., and Zhou, M.F., 2007, Geochemistry of Neoproterozoic mafic intrusions in the Panzhihua district (Sichuan Province, SW China): Implications for subduction related metasomatism in the upper mantle: *Precambrian Research*, v. 152, p. 27–47. [10.1016/j.precamres.2006.09.002](https://doi.org/10.1016/j.precamres.2006.09.002)
- Zhao, J.X., Mcculloch, M.T., and Korsch, R.J., 1994, Characterisation of a plume-related \approx 800 Ma magmatic event and its implications for basin formation in central-southern Australia: *Earth and Planetary Science Letters*, v. 121, no. 3–4, p. 349–367. doi:[10.1016/0012-821X\(94\)90077-9](https://doi.org/10.1016/0012-821X(94)90077-9)
- Zhong, Y., Liu, W.L., Xia, B., Liu, J.N., Guan, Y., Huang, W., and Sun, X.M., 2017, Geochemistry and geochronology of the Mesozoic Lanong ophiolitic mélangé, northern Tibet: Implications for petrogenesis and tectonic evolution: *Lithos*. [in press]. [10.1016/j.lithos.2017.09.003](https://doi.org/10.1016/j.lithos.2017.09.003)
- Zhong, Y., Xia, B., Liu, W.L., Xia, L.Z., Xia, Z.Y., and Wang, L.H., 2013, LA-ICP-MS zircon U-Pb age and genesis of Longbucun granite in Southern Gandise Belt, Tibet: *Geological Bulletin of China*, v. 32, no. 9, p. 1–9. [In Chinese with English abstract.]
- Zhong, Y., Xia, B., Liu, W.L., Yin, Z.X., Hu, X.C., and Huang, W., 2015, Geochronology, petrogenesis and tectonic implications of the Jurassic Namco-Renco ophiolites, Tibet: *International Geology Review*, v. 57, no. 4, p. 508–528. doi:[10.1080/00206814.2015.1017776](https://doi.org/10.1080/00206814.2015.1017776)
- Zhu, D.C., Li, S.M., Cawood, A., Wang, Q., Zhao, Z.D., Liu, S.A., and Wang, L.Q., 2016, Assembly of the Lhasa and Qiangtang terranes in central tibet by divergent double subduction: *Lithos*, v. 245, p. 7–17. [10.1016/j.lithos.2015.06.023](https://doi.org/10.1016/j.lithos.2015.06.023)
- Zhu, D.C., Mo, X.X., Niu, Y., Zhao, Z.D., Wang, L.Q., Liu, Y.S., and Wu, F.Y., 2009, Geochemical investigation of Early Cretaceous igneous rocks along an east-west traverse throughout the central Lhasa Terrane, Tibet: *Chemical Geology*, v. 268, p. 298–312. [10.1016/j.chemgeo.2009.09.008](https://doi.org/10.1016/j.chemgeo.2009.09.008)
- Zhu, D.C., Pan, G.T., Mo, X.X., Wang, L.Q., Zhao, Z.D., Liao, Z.L., Geng, Q.R., and Dong, G.C., 2006, Identification for the Mesozoic OIB-type basalts in central Qinghai-Tibetan Plateau: Geochronology, Geochemistry and their tectonic setting: *Acta Geologica Sinica*, v. 80, no. 9, p. 1312–1328. [In Chinese with English abstract.]
- Zhu, D.C., Pan, G.T., Wang, L.Q., Mo, X.X., Zhao, Z.D., Zhou, C.Y., Liao, Z.L., Dong, G.C., and Yuan, S.H., 2008, Tempo-spatial variations of Mesozoic magmatic rocks in the Gangdese belt, Tibet, China, with a discussion of geodynamic setting-related issues: *Geological Bulletin of China*, v. 27, p. 1535–1550. [In Chinese with English abstract.]
- Zhu, D.C., Zhao, Z.D., Niu, Y., Mo, X.X., Chung, S.L., and Hou, Z. Q., 2011, The Lhasa Terrane: Record of a microcontinent and its histories of drift and growth: *Earth and Planetary Science Letters*, v. 301, p. 241–255. [10.1016/j.epsl.2010.11.005](https://doi.org/10.1016/j.epsl.2010.11.005)
- Zhu, D.C., Zhao, Z.D., Niu, Y.L., Dilek, Y., Hou, Z.Q., and Mo, X. X., 2013, The origin and pre-Cenozoic evolution of the Tibetan Plateau: *Gondwana Research*, v. 23, p. 1430–1455. [10.1016/j.gr.2012.02.002](https://doi.org/10.1016/j.gr.2012.02.002)
- Zhu, Z.Y., 2004, The geochemical characteristics and tectonic setting about ophiolite in Yongzhu-Namcuo: Jilin, Jilin University, p. 1–55. [In Chinese with English abstract.]